CHALMERS
UNIVERSITY OF TECHNOLOGY

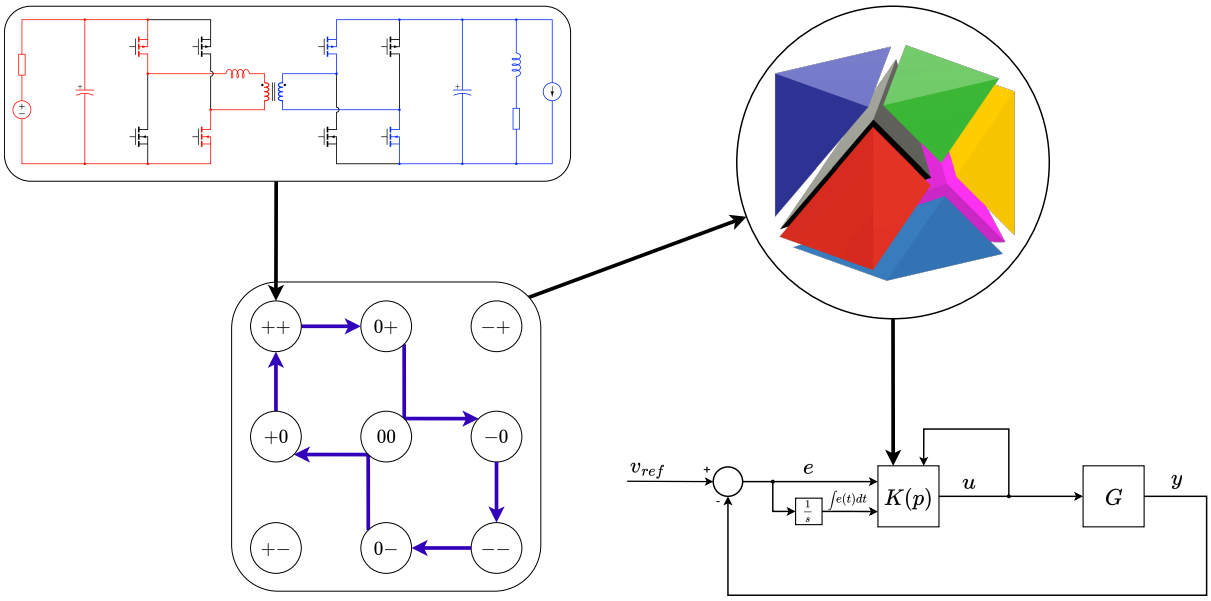

Robust control for TPS DAB converters

Robust LPV MIMO control of phase shifted full-bridge converters with triple phase shift modulation - a state-space modeling approach

Master's thesis in Systems, control and mechatronics

Gustav Abrahamsson, Martin Andersson

Department of Electrical Engineering

CHALMERS UNIVERSITY OF TECHNOLOGY
Gothenburg, Sweden 2024
www.chalmers.se

Master's thesis 2024

Robust control for TPS DAB converters

Robust LPV MIMO control of phase shifted full-bridge converters with triple phase shift modulation - a state-space modeling approach

Gustav Abrahamsson
Martin Andersson

CHALMERS
UNIVERSITY OF TECHNOLOGY

Department of Electrical Engineering
Division of Systems and control
Automatic Control Group
Chalmers University of Technology
Gothenburg, Sweden 2024

Robust control for TPS DAB converters
Robust LPV MIMO control of phase shifted full-bridge converters with triple phase shift modulation - a state-space modeling approach
Gustav Abrahamsson
Martin Andersson

Supervisor: Spyros Gryparis, Aros Electronics & Mebtu Beza, E2
Examiner: Balázs Adam Kulcsár, AC, E2
Mentors: Daniel Chädström, Aros Electronics & Daniel Quach, Aros Electronics

Master's Thesis 2024
Department of Electrical Engineering
Division of Systems and Control
Automatic Control Group
Chalmers University of Technology
SE-412 96 Gothenburg
Telephone +46 31 772 1000

Cover: An illustration of the modeling approach and how the controller is synthesized.

Typeset in LaTeX
Printed by Chalmers Reproservice
Gothenburg, Sweden 2024

Robust control for TPS DAB converters
Robust LPV MIMO control of phase shifted full-bridge converters with triple phase shift modulation - a state-space modeling approach
Gustav Abrahamsson
Martin Andersson
Department of Electrical Engineering
Chalmers University of Technology

Abstract

This thesis investigates the voltage tracking and load disturbance performance of PSFB-DAB DC-DC converters. The main objective of this thesis is to conclude if the selected performance metrics can be improved on, by using more sophisticated controller methods such as model-based robust linear parameter varying controllers. The results show that robust linear parameter-varying controllers can be used to improve the converters' ability to track reference voltages and reject load disturbances. These promising results prove that the necessary model simplifications made still provide usable controllers. Furthermore, it opens up possibilities to explore more complex models where the converters' losses can be modeled and used to synthesize efficiency-maximizing controllers.

Keywords: PSFB, DAB, SPS, TPS, DC-DC, State-space, LPV, Robust control, MIMO.

Acknowledgements

We would like to extend our gratitude to the people who have supported us throughout this thesis. The project would not have gone as far as it did without their patience, commitment, and engagement.

Firstly, we would like to greatly thank Prof. Balázs Adam Kulcsár for his determination to aid us with his expertise in modeling and control.

Secondly, we extend our gratitude to our supervisors Mebtu Beza from Chalmers, and Spyros Gryparis from Aros Electronics for their knowledge in converter theory and implementation.

Thirdly, many thanks to our mentors Daniel Quach and Daniel Chädström at Aros Electronics for the discussions and knowledge regarding converter- and control theory.

Finally, we would like to thank Aros Electronics for providing us with such an interesting and challenging thesis.

Gustav Abrahamsson, Martin Andersson, Gothenburg, June 2024

List of Acronyms

Below is the list of acronyms that have been used throughout this thesis, listed in alphabetical order:

AC	Alternating Current
DC	Direct Current
DAB	Dual Active Bridge
ESR	Equivalent Series Resistance
LPV	Linear Parameter-Varying
LTI	Linear Time-Invariant
MIMO	Multiple Input Multiple Output
MISO	Multiple Input Single Output
MOSFET	Metal-Oxide Semiconductor Field-Effect Transistor
PSFB	Phase Shifted Full Bridge
SISO	Single Input Single Output
SPS	Single Phase Shift
TPS	Triple Phase Shift
ZVS	Zero Voltage Switching

Nomenclature

Below is the nomenclature of parameters, and the variables used in this thesis.

Parameters

R_{in}	Primary voltage source Equivalent Series Resistance
V_{in}	Input voltage
C_1	Primary side DC-link capacitor
C_o	Secondary side DC-link capacitor
L_{load}	Load inductance
R_L	Load resistance
i_{load}	Secondary side current source
A	State matrix
B	Input matrix
C	Output matrix
D	Feedthrough matrix
A_d	Discrete state matrix
B_d	Discrete input matrix
A_{P_d}	Discrete polytope state matrix
B_{P_d}	Discrete polytope input matrix
K_P	Proportional gain
K_I	Integral gain
K_D	Derivative gain
R_{eq}	Equivalent conducting path resistance
R_{MSF}	MOSFET conductive resistance
R_{trafo}	Transformer resistance
$B'_{d,i}$	Discrete linearized input matrix

$\bar{E}_{d,i}$	Constant linearization-point offset
M_k	Polynomial coefficients
$\tilde{D}$	Previous input phase shift
$\bar{u}_i$	Input linearization point
W	Tunable weights
f_s	Switching frequency
T_s	Switching period
T	Controller period

Variables

x	State vector
x_d	Discrete state vector
u	Input vector
y	Output vector
z	Exogenous outputs
w	Exogenous inputs
ϕ	Phase shift between the two bridges
ϕ_1	Primary side phase shift
ϕ_2	Secondary side phase shift
D	Normalized phase shift between primary and secondary bridges
D_1	Primary bridge duty cycle
D_2	Secondary side duty cycle
S_n	Primary side MOSFET gate signals
Q_n	Secondary side MOSFET gate signals
v_p	Primary voltage of transformer
v_s	Secondary voltage of transformer
Δ_m	Model uncertainty
P	Generalized plant
K	Controller
u_Δ	Input perturbation
y_Δ	Output perturbation
i_L	Inductor current
i_o	Output current

v_o	Output voltage
P_n	Polytopes

Contents

List of Acronyms **ix**

Nomenclature **xi**

List of Figures **xvii**

List of Tables **xix**

1 Introduction **1**
1.1 Background . . . 1
1.2 Objective and scope . . . 2
1.3 Limitations . . . 2

2 Theory **3**
2.1 PSFB-DAB converter structure . . . 3
2.1.1 Modulation . . . 3
2.1.2 SPS modulation . . . 4
2.1.3 TPS modulation . . . 4
2.1.4 Dead time . . . 5
2.2 Control theory . . . 5
2.2.1 PID control . . . 5
2.2.2 State-space form . . . 6
2.2.3 Robust control . . . 6
2.2.4 Linear parameter-varying control (LPV) . . . 7

3 Modeling **9**
3.1 SPS modeling . . . 9
3.1.1 Stages . . . 9
3.1.2 Equivalent circuits . . . 10
3.1.3 SPS state-space modeling . . . 12
3.1.4 Averaged model . . . 14
3.1.5 Switching stage model . . . 15
3.1.6 Linearized SPS model . . . 18
3.1.7 Input parametric model . . . 18
3.1.8 Relative error of SPS models . . . 19

3.2 TPS Modeling 20
3.2.1 Equivalent TPS circuits 20
3.2.2 Duration of the TPS stages 22
3.2.3 Order of the TPS stages 23

4 Controller design **31**
4.1 SPS PID 31
4.2 SPS LPV controller 31
4.2.1 TPS LPV controller 34
4.2.2 Auxiliary controller features 35
4.3 Evaluation 36
4.3.1 Performance metrics 37

5 Results **39**
5.1 Tracking and load regulation 39

6 Discussion **45**

7 Conclusion **47**

List of Figures

2.1 Structure of a PSFB DAB DC-DC converter. 3
2.2 SPS waveforms corresponding to $D = 0.5$, $D_1 = 1$ and $D_2 = 1$. 4
2.3 TPS waveforms corresponding to $D = 0.5$, $D_1 = 0.5$ and $D_2 = 0.5$. . . 5
2.4 General Δ-P-K structure. 7

3.1 Stage $\{++\}$. MOSFETs $S1$, $S4$, $Q1$, $Q4$ are conducting. 9
3.2 Stage $\{+-\}$. MOSFETs $S1$, $S4$, $Q2$, $Q3$ are conducting. 10
3.3 Stage $\{-+\}$. MOSFETs $S2$, $S3$, $Q1$, $Q4$ are conducting. 10
3.4 Stage $\{--\}$. MOSFETs $S2$, $S3$, $Q2$, $Q3$ are conducting. 10
3.5 The equivalent circuit for stage $\{++\}$. 11
3.6 The equivalent circuit for stage $\{+-\}$. 12
3.7 The equivalent circuit for stage $\{-+\}$. 12
3.8 The equivalent circuit for stage $\{--\}$. 12
3.9 The voltages v_p (red), v_s (blue) and the durations of each stage in SPS. 14
3.10 The elements of $B_d(D)$. 17
3.11 Relative model error with respect to input frequency for the linearized- and input parametric model. 19
3.12 The equivalent circuit for stage $\{+0\}$. C_o and the load are disconnected from the transformer. 20
3.13 The equivalent circuit for stage $\{-0\}$. Identical to $\{+0\}$, but V_{in} is inverted. 20
3.14 The equivalent circuit for stage $\{0+\}$. Identical to $\{++\}$, but the primary side is disconnected ($V_{in} = 0$). 21
3.15 The equivalent circuit for stage $\{0-\}$. Identical to $\{+-\}$, but the primary side is disconnected ($V_{in} = 0$). 21
3.16 The equivalent circuit for stage $\{00\}$. Identical to $\{+0\}$, but the primary side is disconnected ($V_{in} = 0$). 21
3.17 Primary and secondary voltage waveforms with two different stage orders. 23
3.18 The boundary between two different stage orders defined by $D = D_1 + D_2$. 24
3.19 All boundary planes that intersect with the unit cube. 25
3.20 All polytopes defined by the boundary planes. 26
3.21 An exploded view of the polytopes. 26
3.22 The order of the stages for polytope 5, with initial stage $\{++\}$. . . . 27

3.23 Individual layers of relative error, extracted from the cube. 30

4.1 Δ-P-K structure of the SPS system. 32
4.2 Δ-P-K structure of the TPS system. 34
4.3 The implementation of anti-windup for the SPS LPV controller. . . . 36
4.4 The implementation of anti-windup for the TPS LPV controller. . . . 36
4.5 The voltage tracking and current load scenario. 38

5.1 The complete tracking simulation with all controllers. 39
5.2 The controllers' performance during the first voltage step. 40
5.3 The controllers' performance during the second voltage step. 41
5.4 The controllers' performance during the steps in load current. 42
5.5 The controllers' performance during the final step in reference voltage. 43

List of Tables

3.1 Time spent in each primary side voltage sign. 22
3.2 Time spent in each secondary sign. 23
3.3 Stage order for each polytope 27

4.1 Component values. 37

5.1 Performance metrics for the first voltage step 40
5.2 Performance metrics for the second voltage step. 41
5.3 Performance metrics for the step-up in load current. 42
5.4 Performance metrics for the step-down in load current. 42
5.5 Performance metrics for the step-up in load current. 43

1

Introduction

Along with the electrification of society comes a greater demand for electric power [1]. Loads on the electric infrastructure such as electric vehicles, appliances, and heating are all contributing to ever-growing requirements on the grid. Hence, both generating and transferring such high levels of electrical power to keep up with demands poses a significant engineering challenge.

Maximizing the performance of power electronics is therefore important to both save energy and money. To achieve this, it is often desirable to apply control methods that make power systems operate in regions of minimal losses [2]. However, such control strategies often have room for improvement due to their simplicity, especially for converters with active components and more degrees of freedom.

1.1 Background

The usage of Dual Active Bridge (DAB) converters has increased in recent years due to their efficiency and versatility [3]. Traditional converters often extensively utilize diodes, which in most cases pose significant losses at high power. Decreasing the losses from the inevitable voltage dropouts caused by the diodes' threshold voltage can be mitigated by using higher-quality components. This is something that increases the cost of the converter, which is not preferable. By avoiding such diodes and opting for actively controlling MOSFET:s in full bridges, the losses can be reduced [4].

The DAB converter topology uses a high frequency transformer to isolate the two DC links [5]. This provides certain benefits, such as protection against voltage spikes and electrical noise. Undesired current flow between the DC links can be prohibited, while the safety of the converter can be increased. The added components needed for isolation does however result in higher component costs [6].

DAB converters enable different control methods, with varying degrees of freedom. Single Phase Shift (SPS) operation is one of the most simple control strategies, and Triple Phase Shift (TPS) modulation enables higher efficiency due to the possibility of Zero Voltage Switching (ZVS) [7].

This increases the potential for the converter's performance, but poses a greater challenge in terms of control. Having more control signals available increases the degrees of freedom in terms of affecting the converter, at the cost of having to use more advanced model-based control strategies [8].

The focus of this thesis is to analyze the dynamics and implement a robust controller for a Phase-Shifted Full Bridge (PSFB) Dual-Active Bridge DC-DC converter using TPS- and SPS modulation.

1.2 Objective and scope

This thesis aims to investigate how well different controllers can track a reference in the output voltage of the converter with an unknown- and variable load. In this thesis, the number of investigated controllers will be limited to PID- and Linear Parameter-Varying (LPV) controllers.

To be able to investigate the LPV controllers, models of the converter need to be derived and evaluated, from which the controllers then can be synthesized. Evaluation of these controllers will be done only with simulations and not on hardware.

1.3 Limitations

The controllers will only be evaluated on voltage tracking performance and load disturbance rejection. Performance metrics such as losses in the converter will not be estimated nor analyzed.

The load will be modelled as a nominal resistive and inductive load with an additional varying current load in parallel. This structure captures the behavior of most loads relevant to this converter type.

2

Theory

In this chapter, the relevant theory will be presented. The functionality of the converter in question will be explained, as well as the underlying control theory for the proposed controllers.

2.1 PSFB-DAB converter structure

The PSFB-DAB converter has a symmetric topology that consists of two active full bridges connected through a transformer [9]. A schematic illustrating this is shown in Fig 2.1. High frequency switching of the MOSFETs in each full bridge enables conversion from DC to AC, and back to DC [9]. Furthermore, the symmetric topology enables bidirectional power transfer through the converter.

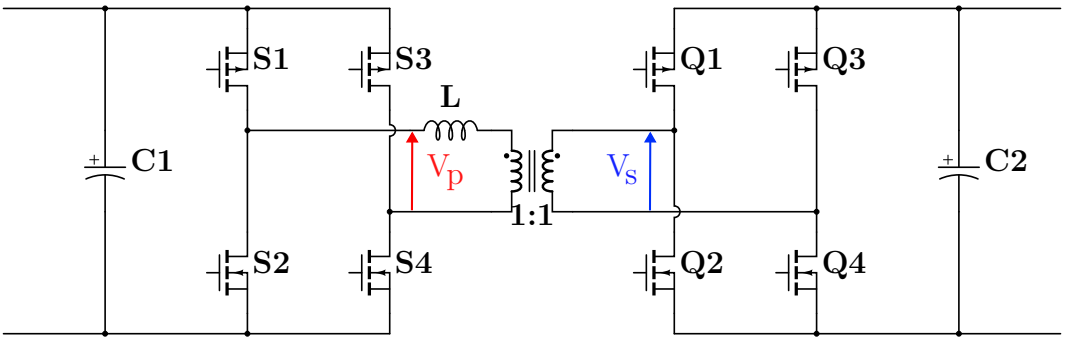

Figure 2.1: Structure of a PSFB DAB DC-DC converter.

2.1.1 Modulation

While the switching frequency of the MOSFET:s is fixed, the phase shifts between some of them are adjustable. These are the three phase shifts ϕ, ϕ_1, and ϕ_2 which affect the modulation of the switching signals.

The control signal ϕ changes the phase shift between the two full bridges. It is defined as the phase shift between the gate signals applied to the S1 and Q1 MOSFET:s. It is bounded to $\pm 90°$ (the sign decides power flow direction), but bi-directional

power flow will not be investigated. Hence, the normalized phase shift $D \in [0,\ 1]$ corresponds to $[0°,\ 90°]$.

The remaining ϕ_1 and ϕ_2 change the phase shift between the two legs in the primary ($S1$ and $S4$) and secondary ($Q1$ and $Q4$) bridges respectively. This effectively means that the phase shift ratio in each bridge can be controlled [7]. Another way of interpretation this, is to view these phase shifts as duty cycles $D_1, D_2 \in [0,\ 1]$ of the output voltage from each bridge. Similarly to ϕ, these normalized versions will be used when modeling the system.

Additionally, these phase shifts are limited in how fast they can be changed. The given limits for this converter modulation scheme restricts D, D_1 and D_2 to a rate limit of ± 0.2 per sample at 25 kHz switching frequency.

2.1.2 SPS modulation

The simplest way to control the converter is through SPS modulation, which only uses D to control the converter while fixing $D_1 = D_2 = 1$. An example of the waveforms created when the converter is operated with SPS control is shown in Fig 2.2 where v_p and v_s are the primary and secondary voltages of the transformer.

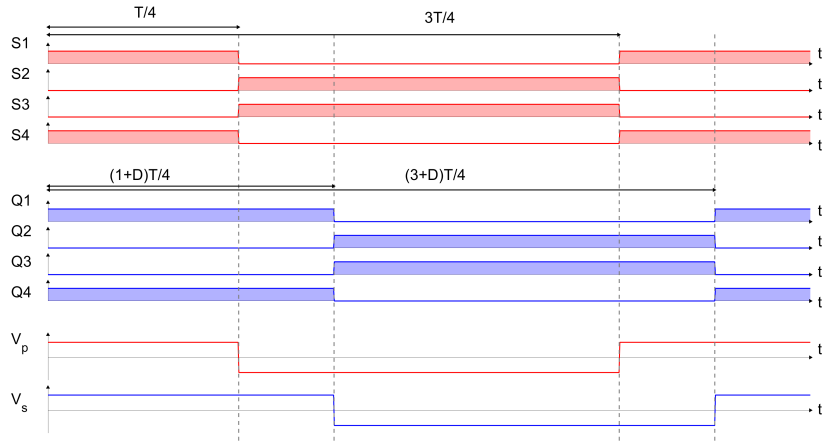

Figure 2.2: SPS waveforms corresponding to $D = 0.5$, $D_1 = 1$ and $D_2 = 1$.

While it is more convenient to only have one control variable available, it limits the potential of the converter [7].

2.1.3 TPS modulation

The most complex modulation approach is TPS modulation, which utilizes all available control variables D, D_1 and D_2. An example of the waveforms created when the converter is operated with TPS control is shown in Fig 2.3.

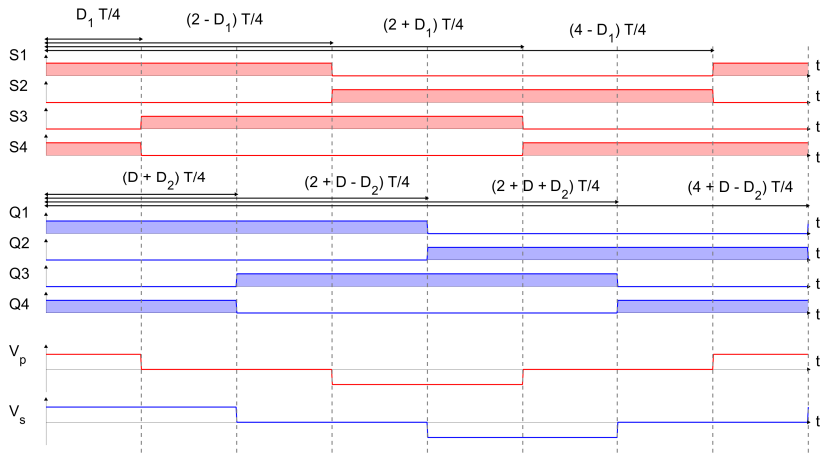

Figure 2.3: TPS waveforms corresponding to $D = 0.5$, $D_1 = 0.5$ and $D_2 = 0.5$.

2.1.4 Dead time

The dead time of the converter is the time between when one leg of a bridge turns off and when the other leg turns on. The converter must operate with some amount of dead time to avoid creating a short circuit on either the primary or secondary side [10].

2.2 Control theory

This section will provide the basic theoretical background necessary to understand the controllers implemented in this thesis.

2.2.1 PID control

Proportional Integral Derivative (PID) controllers are the most widely used controllers due to how simple they are to implement and how well they can manage to stabilize and control various systems. They can be implemented without a mathematical model of the system being required. The PID controller is a Single Input Single Output (SISO) controller with its input signal being an error signal $e(t)$ which is computed as the difference between the reference and the measured value. The output of the PID controller u is computed according to equation (2.1).

$$u = K_P \cdot e(t) + K_I \cdot \int_0^t e(\tau)d\tau + K_D \cdot \frac{d}{dt}e(t) \tag{2.1}$$

The K_P term relates to how drastically the controller reacts to the measured error. Increasing K_P will result in a faster but less stable controller. The K_I term relates to how the controller output depends on the integral of the error, where increasing

K_I results in a controller that minimizes steady-state errors, but that's less stable and more prone to cause an oscillatory behavior. The K_D term relates to how the controller output depends on the derivative of the error. Increasing the K_D term increases stability but will make the controller sensitive to measurement noise.

2.2.2 State-space form

A system can be represented in state-space if it is a linear time-invariant system (LTI). For control purposes, modeling systems on state-space form have many benefits, mainly that it provides a solid framework on which the systems can be analyzed where controllers can be designed systematically [11]. $x(t) \in \mathcal{R}^{n\times 1}$ is a column vector containing the states of the system, $u(t) \in \mathcal{R}^{m\times 1}$ describes the inputs, while $y(t) \in \mathcal{R}^{k\times 1}$ is the output. A model on state-space form consists of matrices $A \in \mathcal{R}^{n\times n}$, $B \in \mathcal{R}^{n\times m}$, $C \in \mathcal{R}^{k\times n}$ and $D \in \mathcal{R}^{k\times m}$ as shown in equation (2.2). The state-space form of a system is easily obtained if the dynamics of the system are known, as the state-space form is a system of first order differential equations written on matrix form.

$$\begin{aligned} \dot{x}(t) &= Ax(t) + Bu(t) \\ y(t) &= Cx(t) + Du(t) \end{aligned} \tag{2.2}$$

State-space models are often used when modeling Multiple Input Multiple Output (MIMO) systems and can also be used to design MIMO controllers.

2.2.3 Robust control

Most control design methods assume that the model of the plant is a perfect representation of the real plant. Robust control theory provides the tools necessary to model additional uncertainties such as measurement noise, plant disturbances and model uncertainties in a way that makes the controller aware of these uncertainties. The robust model structure is shown in Fig 2.4 where the Δ function represents uncertainties in the model. It is assumed to be bounded, and that $||\Delta||_\infty < 1$. The P block is the generalized plant block which contains the plant along with potential weights used to tune the system, and the K is the controller of the system.

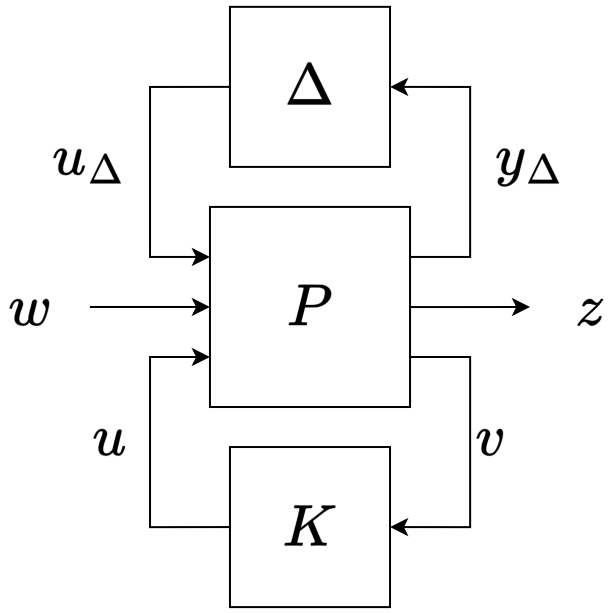

Figure 2.4: General Δ-P-K structure.

The controller K is chosen in such a way that the gain from the disturbances w to the performance metrics z is minimized [12]. Examples of disturbances are reference signals, measurement noise and process noise. The performance metrics are set in such a way that they reflect the desired behavior of the controller. Examples of performance metrics could be tracking errors z_e or control signal usage z_u. Potential weights in the form of transfer functions can be used to alter the controller's response to certain signals depending on their frequency. For instance, if low control signal activity is desired, a high-pass filter as weight W_u will penalize high frequency signals. This results in amplification of high frequent control signal usage, thus discouraging the controller from using high frequency control signals.

The gain from w to z can be minimized in different ways. The two most commonly used system norms are the $\mathcal{H}_2$ and $\mathcal{H}_\infty$ norms. The $\mathcal{H}_2$ norm takes the gain at all frequencies into account, whereas the $\mathcal{H}_\infty$ norm only focuses on peak gain. These two different ways of computing the gain influences the behavior of the controller. Using the $\mathcal{H}_2$ norm will result in a controller that seeks to minimize the effects of the disturbances for all frequencies, while the $\mathcal{H}_\infty$ norm seeks to minimize the worst case gain.

2.2.4 Linear parameter-varying control (LPV)

LPV controllers are used for systems that have a linear parameter dependency. The varying system matrices of a LPV system poses challenges when synthesizing controllers. An option to solve this, is to schedule the model at various operating points based on measured parameter values. This approach results in numerous linear controllers only valid for specific parameter values. The generated control signal is an output of a system interpolated between multiple controllers in the

vicinity of the current parameter values.

In this thesis, the MATLAB toolbox LPVTools [13] is used. This toolbox provides the tools and functions necessary to model and synthesize robust controllers for LPV systems. Given bounds on the parameter values and their derivatives, LPVTools features functions that synthesize robust controllers. This is performed such that the given system is stable in every point, while also minimizing the $\mathcal{L}_2$ norm. Potential parameter changes are taken into account by the previously stated parameter derivative bounds.

3

Modeling

A requirement set on the model, is that it must be possible to synthesize controllers with frequencies equal to the switching frequency of the MOSFETs. This is due to the limit in control loop frequency.

3.1 SPS modeling

In this section, the derivations for the SPS model are presented.

3.1.1 Stages

The bridges can directly apply, invert, or disconnect their respective voltages on the transformer, creating the wave forms of the primary and secondary voltages v_p and v_s. These voltages are therefore modelled as either positive, zero, or negative, which will from now on be referred to as '+', '0', and '−' respectively.

The different combinations of $\{v_p, v_s\}$ during SPS modulation are therefore labeled $\{++\}$, $\{+-\}$, $\{-+\}$, and $\{--\}$, and will be referred to as 'stages'. For simplicity, the conducting behavior of the body diodes is neglected. Illustrations of these stages are shown in Fig 3.1 to 3.4.

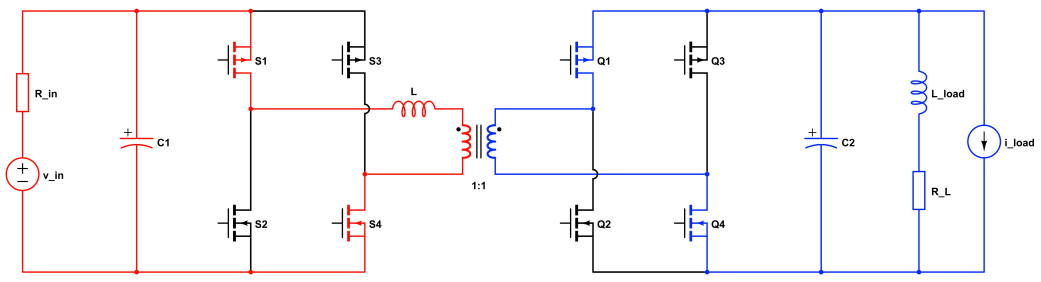

Figure 3.1: Stage $\{++\}$. MOSFETs $S1$, $S4$, $Q1$, $Q4$ are conducting.

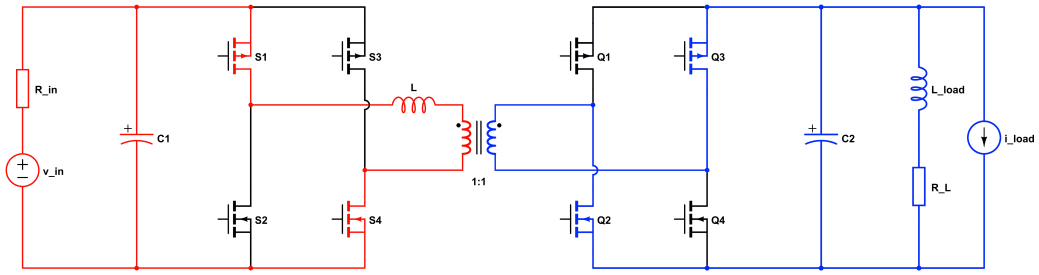

Figure 3.2: Stage $\{+-\}$. MOSFETs $S1$, $S4$, $Q2$, $Q3$ are conducting.

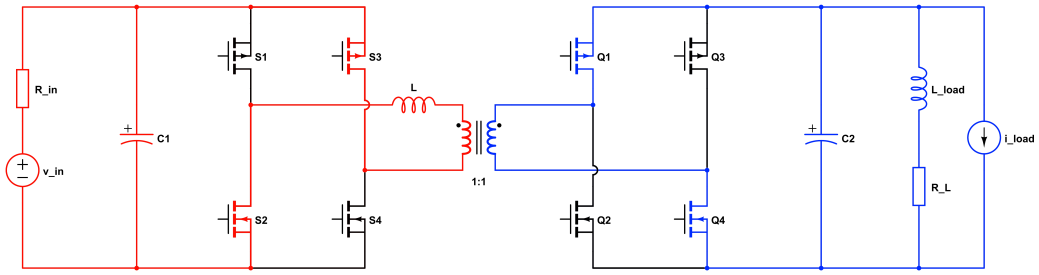

Figure 3.3: Stage $\{-+\}$. MOSFETs $S2$, $S3$, $Q1$, $Q4$ are conducting.

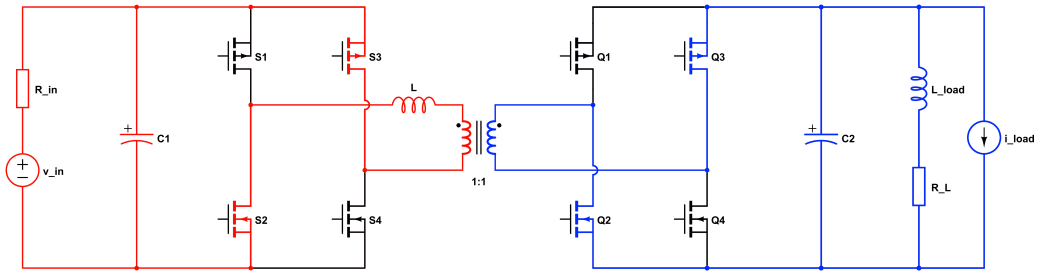

Figure 3.4: Stage $\{--\}$. MOSFETs $S2$, $S3$, $Q2$, $Q3$ are conducting.

3.1.2 Equivalent circuits

Each stage can be expressed as its own equivalent circuit without active components. This is because each stage is representing the converter given a combination of switch states. The usage of model error compensation in the controller will enable the following approximations to generate a model sufficiently accurate for control synthesis.

The transformer has a winding ratio of 1:1, and the magnetizing inductance of the transformer L_{mag} is considerably larger than the leakage inductance L. The model in this thesis can then be simplified as merely the leakage inductance, resistance (R_{trafo}) and a direct coupling between the two bridges.

The MOSFET:s are therefore replaced with their conducting resistances. The equivalent resistance R_{eq} is then approximated to be equal to the primary voltage source equivalent series resistance (ESR), conducting resistance of the MOSFET:s and conducting resistance of the transformer, namely

$$R_{eq} = R_{in} + 4R_{MSF} + R_{trafo}. \tag{3.1}$$

Furthermore, dynamics posed by the parasitic capacitance of the MOSFET:s are negligible for this model, and will therefore not be represented in the equivalent circuit.

The DC-link capacitor on the primary side (C_1) is neglected due to it not being necessary for this thesis' purposes. Adding it will increase the order of the model, but not add valuable information. The voltage over C_1 will be stable during operation, i.e. that $v_{C_1} \approx V_{in}$, with the assumption that the true source voltage is able to supply the rated amount of current. V_{in} in the equivalent circuit is then assumed to be constant.

The equivalent circuits for all SPS stages are illustrated in Fig 3.5 - 3.8.

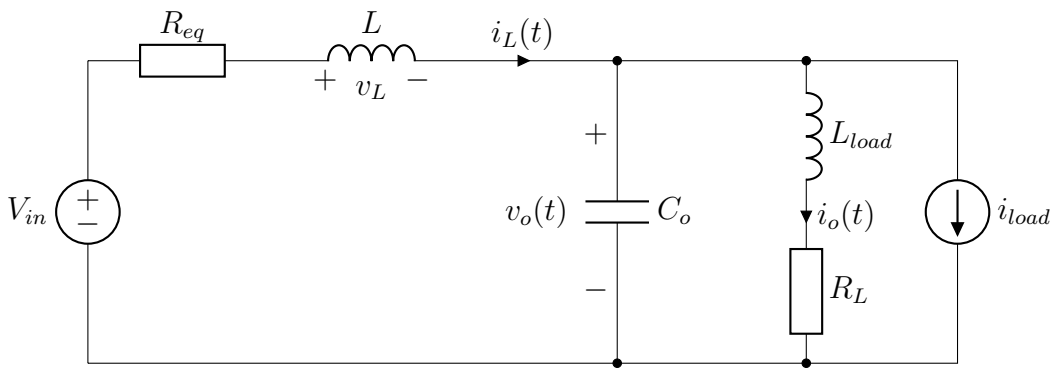

Figure 3.5: The equivalent circuit for stage {++}.

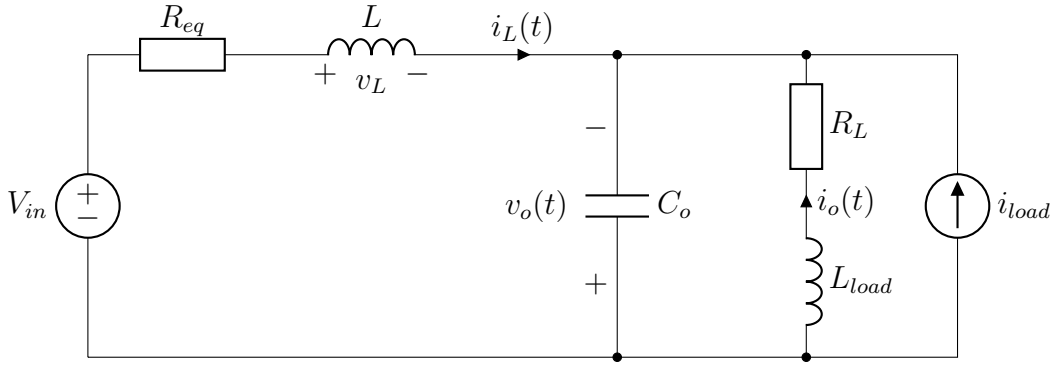

Figure 3.6: The equivalent circuit for stage {+−}.

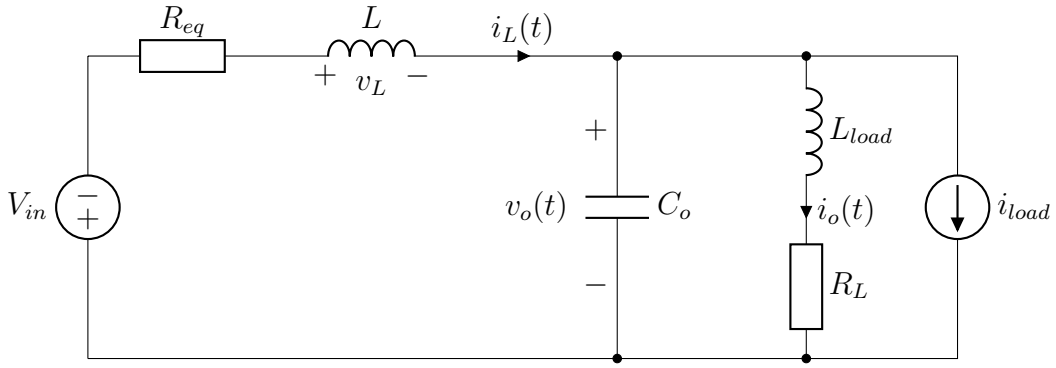

Figure 3.7: The equivalent circuit for stage {−+}.

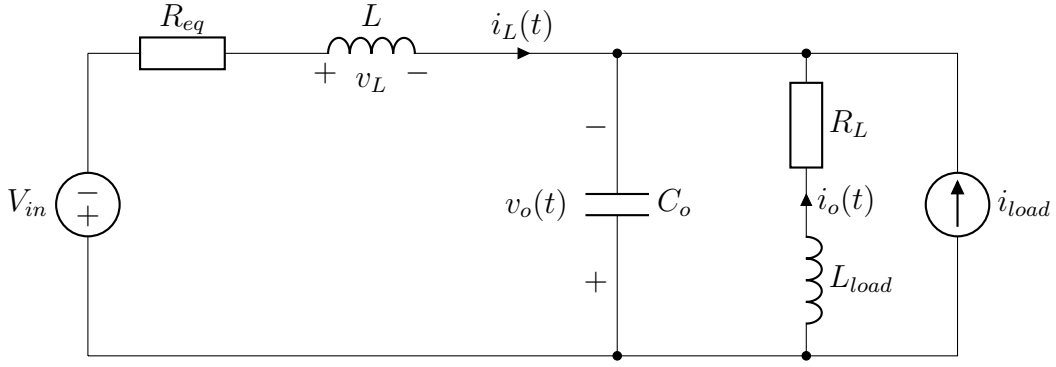

Figure 3.8: The equivalent circuit for stage {−−}.

3.1.3 SPS state-space modeling

All the derived equivalent circuits are constructed with passive components, and can thereby be modeled as continuous LTI state-space models. The time-varying state vector x consists of inductor current i_L, output current i_o and output voltage v_o. The input u is composed of converter input voltage V_{in} and load disturbance i_{load}. While $V_{in} \in [550\ V,\ 850\ V]$, it is assumed to be constant. Additionally, all

component values in the circuit are assumed to be constant. These models are shown in equations (3.2) - (3.6).

$$x = \begin{bmatrix} i_L \\ i_o \\ v_o \end{bmatrix}, \qquad u = \begin{bmatrix} V_{in} \\ i_{load} \end{bmatrix} \tag{3.2}$$

$$A_{\{++\}} = \begin{bmatrix} \frac{-R_{eq}}{L} & 0 & \frac{-1}{L} \\ 0 & \frac{-R_L}{L_{load}} & \frac{1}{L_{load}} \\ \frac{1}{C_o} & \frac{-1}{C_o} & 0 \end{bmatrix}, \qquad B_{\{++\}} = \begin{bmatrix} \frac{1}{L} & 0 \\ 0 & 0 \\ 0 & \frac{-1}{C_o} \end{bmatrix} \tag{3.3}$$

$$A_{\{+-\}} = \begin{bmatrix} \frac{-R_{eq}}{L} & 0 & \frac{1}{L} \\ 0 & \frac{-R_L}{L_{load}} & \frac{1}{L_{load}} \\ \frac{-1}{C_o} & \frac{-1}{C_o} & 0 \end{bmatrix}, \qquad B_{\{+-\}} = \begin{bmatrix} \frac{1}{L} & 0 \\ 0 & 0 \\ 0 & \frac{-1}{C_o} \end{bmatrix} \tag{3.4}$$

$$A_{\{-+\}} = \begin{bmatrix} \frac{-R_{eq}}{L} & 0 & \frac{-1}{L} \\ 0 & \frac{-R_L}{L_{load}} & \frac{1}{L_{load}} \\ \frac{1}{C_o} & \frac{-1}{C_o} & 0 \end{bmatrix}, \qquad B_{\{-+\}} = \begin{bmatrix} \frac{-1}{L} & 0 \\ 0 & 0 \\ 0 & \frac{-1}{C_o} \end{bmatrix} \tag{3.5}$$

$$A_{\{--\}} = \begin{bmatrix} \frac{-R_{eq}}{L} & 0 & \frac{1}{L} \\ 0 & \frac{-R_L}{L_{load}} & \frac{1}{L_{load}} \\ \frac{-1}{C_o} & \frac{-1}{C_o} & 0 \end{bmatrix}, \qquad B_{\{--\}} = \begin{bmatrix} \frac{-1}{L} & 0 \\ 0 & 0 \\ 0 & \frac{-1}{C_o} \end{bmatrix} \tag{3.6}$$

For SPS, the only time the v_p or v_s voltages are zero is during dead time, but this is omitted for this SPS model. To create a model that can be used for control synthesis, these four models need to be combined into one unified model.

During SPS-operation, the only control variable available is the phase-shift (D) between the full bridges. It is also determining the duration which is spent in each of the four stages during a switching period. Its maximum value is 1, which corresponds to a quarter of the switching period. This is illustrated in Fig 3.9.

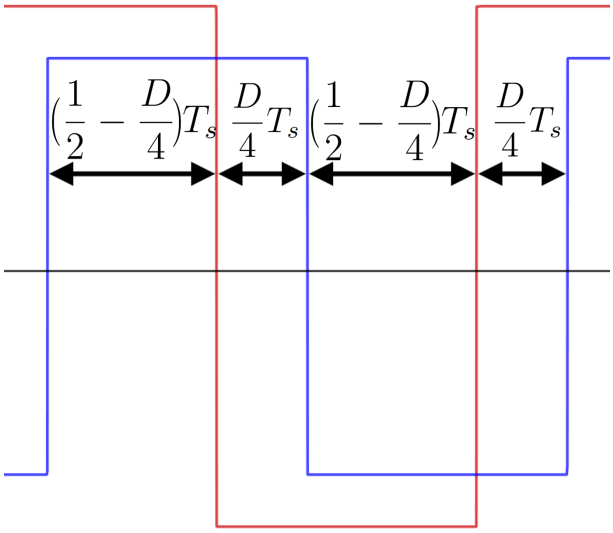

Figure 3.9: The voltages v_p (red), v_s (blue) and the durations of each stage in SPS.

In this thesis, the desired sampling period of the model T (the given control loop period) corresponds with the switching period of the converter T_s, hence

$$T = T_s. \tag{3.7}$$

These durations are then labeled according to equation (3.8).

$$t_{\{++\}} = (\frac{1}{2} - \frac{D}{4})T, \quad t_{\{-+\}} = \frac{D}{4}T, \quad t_{\{--\}} = (\frac{1}{2} - \frac{D}{4})T, \quad t_{\{+-\}} = \frac{D}{4}T \tag{3.8}$$

These durations are defined as the time spent in each stage, and the sum represents the time before returning to the same stage again, which explains why $t_{\{++\}}+t_{\{-+\}}+t_{\{--\}}+t_{\{+-\}} = T$ regardless of D.

3.1.4 Averaged model

One way to condense these state-space models into one, is to average over one switching period. This method does however result in an unusable model since the averaged B_{avg} matrix only contains zeroes in the first column.

$$B_{avg} = \frac{B_{\{++\}} \cdot t_{\{++\}} + B_{\{-+\}} \cdot t_{\{-+\}} + B_{\{--\}} \cdot t_{\{--\}} + B_{\{+-\}} \cdot t_{\{+-\}}}{T}$$

$$= \begin{bmatrix} 0 & 0 \\ 0 & 0 \\ 0 & -\frac{1}{C_o} \end{bmatrix} \tag{3.9}$$

This means that the input voltage has no influence over the output voltage, which it has in reality. This approach of modeling is therefore not a viable option, since it does not adequately capture the behavior of the converter.

3.1.5 Switching stage model

In this thesis the proposed approach is that every stage is modeled as a step of a discrete state-space model. Similar existing research have presented such models, but have ended up with elements in the matrices that switch during a switching period [14]. This thesis presents a model where the sampling time T is chosen as the converter switching frequency T_s, to avoid any discontinuous model switching. This allows for an entire switching period to be modeled as one complete discrete step, by evaluating the four consecutive stages with their respective durations depending on D. To enable this, each state-space matrix in equations (3.3) - (3.6) is discretized according to equation (3.10).

$$A_d = e^{At}, \quad B_d = A^{-1}(A_d - I)B \tag{3.10}$$

Given the state vector x_n (at sample index n), all stages can be compiled into one complete step to x_{n+1} by evaluating each stage consecutively. Assuming that the initial stage is $\{++\}$ (x_n is precisely when stage $\{++\}$ starts), and that the input u_n is constant over one switching period, the following expressions are produced. Note that e.g. $x_{d\{++\}}$ signifies the state vector once stage $\{++\}$ has been evaluated.

$$x_{d\{++\}} = A_{d\{++\}}x_n + B_{d\{++\}}u_n \tag{3.11}$$

$$x_{d\{-+\}} = A_{d\{-+\}}\left(A_{d\{++\}}x_n + B_{d\{++\}}u_n\right) + B_{d\{-+\}}u_n \tag{3.12}$$

$$x_{d\{--\}} = A_{d\{--\}}\left(A_{d\{-+\}}\left(A_{d\{++\}}x_n + B_{d\{++\}}u_n\right) + B_{d\{-+\}}u_n\right) + B_{d\{--\}}u_n \tag{3.13}$$

$$x_{n+1} = x_{d\{+-\}} = \tag{3.14}$$
$$A_{d\{+-\}}\left(A_{d\{--\}}\left(A_{d\{-+\}}\left(A_{d\{++\}}x_n + B_{d\{++\}}u_n\right) + B_{d\{-+\}}u_n\right) + B_{d\{--\}}u_n\right) + B_{d\{+-\}}u_n$$

The following sample x_{n+1} in the model is chosen as the state vector when stage $\{+-\}$ is evaluated. This is because the end of stage $\{+-\}$ is the start of stage $\{++\}$. Its formula (3.14) can be rewritten by separating x_n and u_n to extract the complete matrices $A_d(D)$ and $B_d(D)$.

$$x_{n+1} = \underbrace{(A_{d\{+-\}}A_{d\{--\}}A_{d\{-+\}}A_{d\{++\}})}_{A_d(D)}x_n + \tag{3.15}$$
$$+\underbrace{(B_{d\{+-\}} + A_{d\{+-\}}B_{d\{--\}} + A_{d\{+-\}}A_{d\{--\}}B_{d\{-+\}} + A_{\{+-\}}A_{d\{--\}}A_{d\{-+\}}B_{d\{++\}})}_{B_d(D)}u_n.$$

The combined discrete model is then given by

$$x_{n+1} = A_d(D)x_n + B_d(D)u_n, \quad u_n = \begin{bmatrix} V_{in} \\ i_{load} \end{bmatrix}. \tag{3.16}$$

The fact that $u_n = [V_{in} \quad i_{load}]^T$ makes it unsuitable for control synthesis, which calls for reformatting of the model. This is because the input to the model has to be expressed in terms of the available control variables, which is D for SPS. This means that a change of variables is needed, such that D becomes the input to the system and V_{in} becomes a parameter in the model. To achieve this, the matrices' D dependency must be analyzed and adapted such that the model can be written on the form

$$x_{n+1} = A_d(D)x_n + B_d(V_{in})u_n \ , \quad u = \begin{bmatrix} D \\ i_{load} \end{bmatrix}. \tag{3.17}$$

Note that

$$\frac{\partial B_d(V_{in})}{\partial V_{in}} = 1 \tag{3.18}$$

i.e. that the dependency of V_{in} is merely linear, which means that V_{in} is in practice linearly scaling the B-matrix of the system. This is because it is a linear input to the previous system in equation (3.17).

Evaluating the A-matrix of this system gives

$$A_d(D) = A_{d\{+-\}}A_{d\{--\}}A_{d\{-+\}}A_{d\{++\}} =$$
$$= e^{A_{\{+-\}}(\frac{D}{4}T)}e^{A_{\{--\}}\left((\frac{1}{2}-\frac{D}{4})T\right)}e^{A_{\{-+\}}(\frac{D}{4}T)}e^{A_{\{++\}}\left((\frac{1}{2}-\frac{D}{4})T\right)} \tag{3.19}$$

The chosen stage order aligns the A-matrices in such a way that the D-dependency cancels out when the symmetries $A_{\{+-\}} = A_{\{--\}}$ and $A_{\{++\}} = A_{\{-+\}}$ from equations (3.3) - (3.6) are applied [14]. Hence,

$$\begin{aligned} A_d(D) &= e^{A_{\{--\}}(\frac{D}{4}T)} e^{A_{\{--\}}\left((\frac{1}{2}-\frac{D}{4})T\right)} e^{A_{\{++\}}(\frac{D}{4}T)} e^{A_{\{++\}}\left((\frac{1}{2}-\frac{D}{4})T\right)} \\ \therefore\ A_d &= e^{A_{\{--\}}(\frac{T}{2})} e^{A_{\{++\}}(\frac{T}{2})} \\ \frac{\partial A_d}{\partial D} &= 0. \end{aligned} \tag{3.20}$$

The D dependency of $B_d(D)$ was examined using MATLAB with Symbolic Toolbox [15] due to its complexity. Each element of $B_d(D)$ for $D \in [0,\ 1]$ is shown in Fig 3.10.

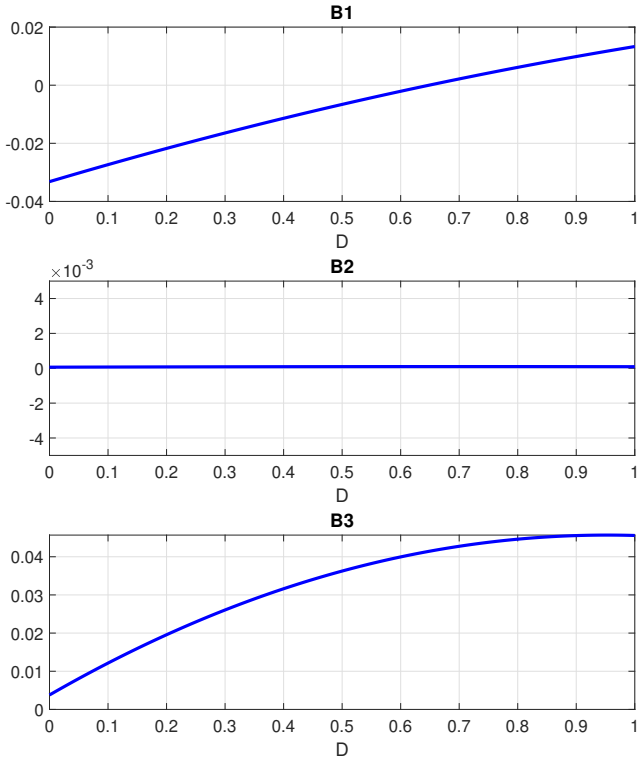

Figure 3.10: The elements of $B_d(D)$.

This means that the phase shift has a non-linear effect on the system and thus cannot be expressed as an LTI system.

3.1.6 Linearized SPS model

A possible solution to the fact that D is not a linear input, is by linearizing $B_d(D)$ with respect to D. Note that this is not linearization around equilibirum points, and merely for changing control inputs. This results in multiple linear models that are scheduled by D. Additionally, V_{in} is included in the new B-matrix as a parameter.

$$B_d(D) \approx \underbrace{\left.\frac{\partial(B_d(D)V_{in})}{\partial D}\right|_{\bar{D}_i}}_{B'_{d,i}} (D - \bar{D}_i) + B_d(\bar{D}_i)V_{in}$$

$$= B'_{d,i}D - \underbrace{(B'_{d,i}\bar{D}_i - B_d(\bar{D}_i)V_{in})}_{\bar{E}_{d,i}} \tag{3.21}$$

$$= [B'_{d,i} \quad -\bar{E}_{d,i}] \underbrace{\begin{bmatrix} D \\ 1 \end{bmatrix}}_{u'} \tag{3.22}$$

When the model is used (either for simulation or control), the value of D at sample n is not available at sample n, which means that it can not be used as a scheduling parameter. Instead, the previous input $\tilde{D} = D_{n-1}$, can be used. Due to the fact that D is rate limited, there is a maximum bound on how incorrect this assumption is.

3.1.7 Input parametric model

Another approach is to extract a single D term from each B_d element, and use the extracted D term as the input to the system. Then, treat all remaining D terms still in the B matrix as known parameters, which get evaluated with the previous input value. Similarly to the linearized model, V_{in} is included in $B_d(D)$. This approach is viable since $B_d(D)$ can be expressed as a polynomial in D, hence

$$B_d(D) = B_d(0) + M_1 D + M_2 D^2 + M_3 D^3 + \ldots + M_n D^n\,, \qquad M_k \in \mathbb{R}^3. \tag{3.23}$$

By extracting D from the terms that include it, and defining the constant offset $\bar{B}_d = B_d(0)$, $B_d(D)$ can be written on the following form

$$B_d(D) = \underbrace{(M_1 + M_2 D + M_3 D^2 + \ldots + M_n D^{n-1})}_{\tilde{B}_d(D)} D + \bar{B}_d$$

$$= \tilde{B}_d(D)D + \bar{B}_d \tag{3.24}$$

Similarly to the linearized model, the value of D from the previous sample ($\tilde{D}$) can be used as a parameter.

$$B_d(D) = \tilde{B}_d(\tilde{D})D + \bar{B}_d \tag{3.25}$$

This approach allows for a single model to be used, as opposed to the several needed with the linearization approach. The accuracy of the model is however dependent on control input usage, as this method assumes that the input to the system in the previous switching period is the same as the input applied to the system at the current switching period.

3.1.8 Relative error of SPS models

Both the linearized- and input parametric models were compared with a Simscape electrical [16] model of the system, which was used to evaluate their accuracy. By sweeping between 15 Hz and 15 kHz and computing the mean relative error, frequency dependent error can be obtained. The specified range is chosen to capture most frequencies of the control input during operation. This is displayed in Fig 3.11.

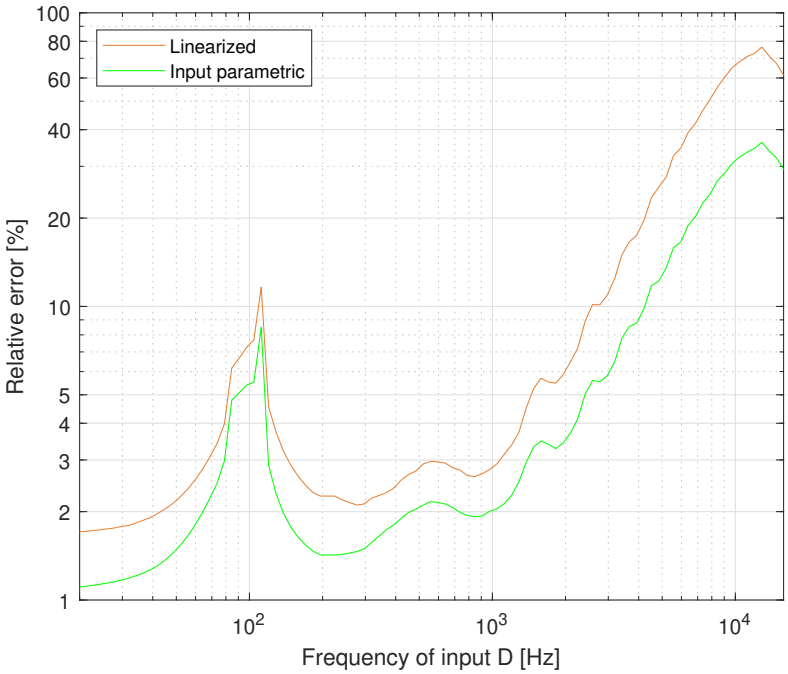

Figure 3.11: Relative model error with respect to input frequency for the linearized- and input parametric model.

3.2 TPS Modeling

To derive a TPS model of the system, a similar approach for the SPS model was used. The additional control variables D_1 and D_2 open up the possibility for the converter to operate in additional stages than the four available for the SPS model. These additional stages arise due to that the primary- and secondary voltages now can arrive in the '0' state. This means that there are 5 new possible stages for TPS modulation when compared to SPS.

3.2.1 Equivalent TPS circuits

The new stages in question are $\{+0\}$, $\{-0\}$, $\{0+\}$, $\{0-\}$, $\{00\}$, and their respective equivalent circuits are shown in Figs 3.12 - 3.16.

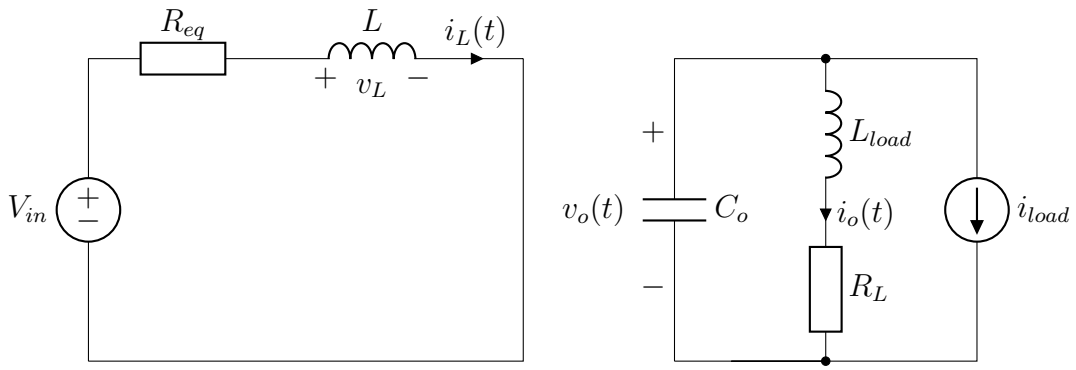

Figure 3.12: The equivalent circuit for stage $\{+0\}$. C_o and the load are disconnected from the transformer.

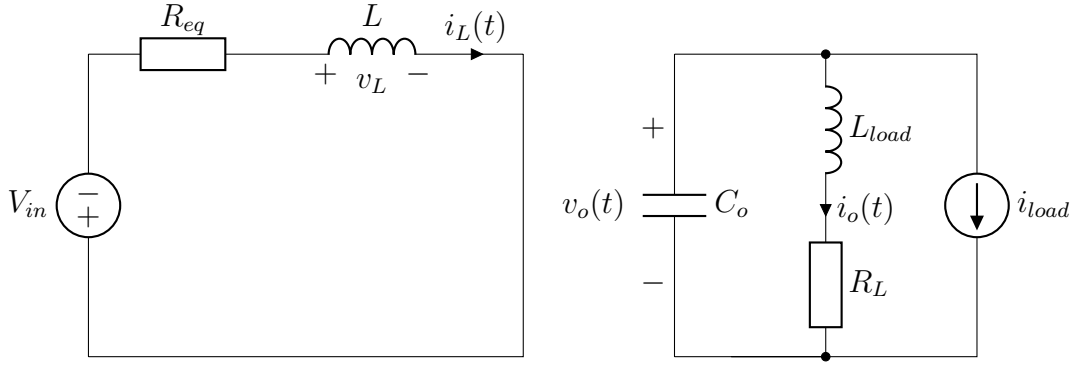

Figure 3.13: The equivalent circuit for stage $\{-0\}$. Identical to $\{+0\}$, but V_{in} is inverted.

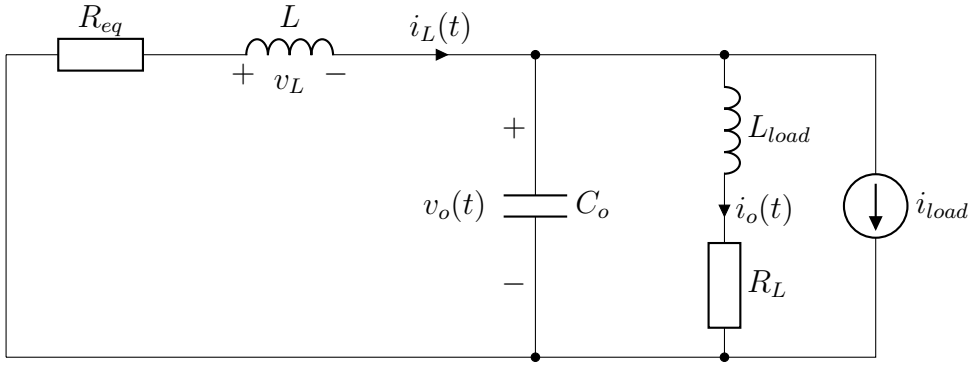

Figure 3.14: The equivalent circuit for stage {0+}. Identical to {++}, but the primary side is disconnected ($V_{in} = 0$).

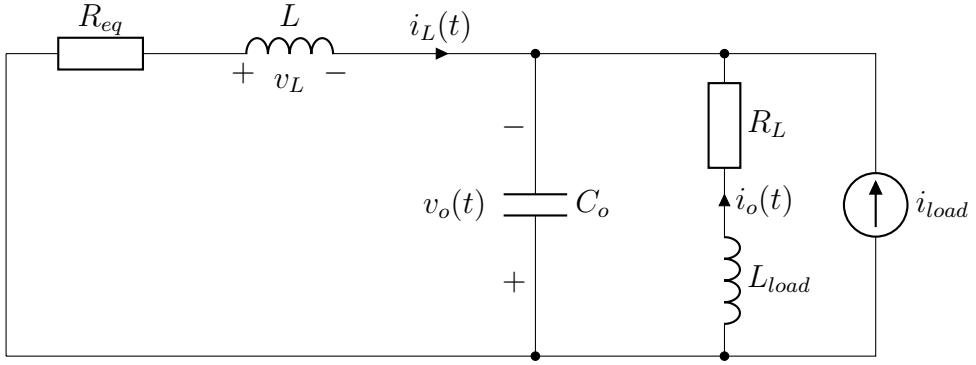

Figure 3.15: The equivalent circuit for stage {0−}. Identical to {+−}, but the primary side is disconnected ($V_{in} = 0$).

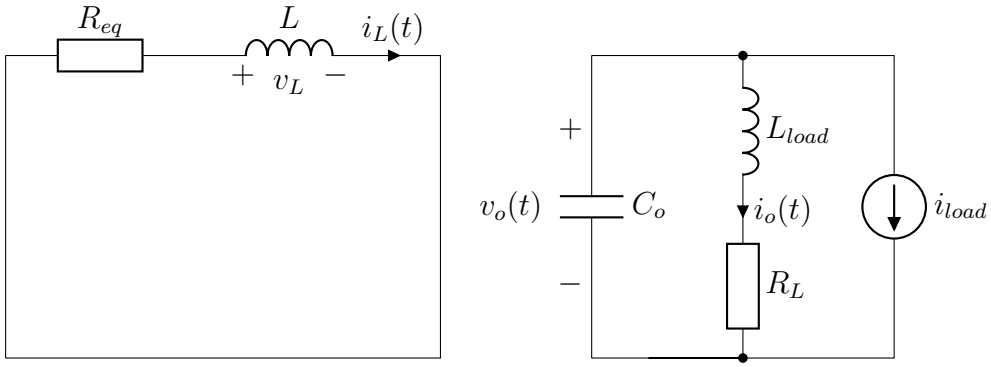

Figure 3.16: The equivalent circuit for stage {00}. Identical to {+0}, but the primary side is disconnected ($V_{in} = 0$).

The circuits are still solely composed of passive components, which means that state-space models can be derived from each one of them. These are shown in equations (3.26) – (3.30).

$$A_{\{+0\}} = \begin{bmatrix} \frac{-R_{eq}}{L} & 0 & 0 \\ 0 & \frac{-R_L}{L_{load}} & \frac{1}{L_{load}} \\ 0 & \frac{-1}{C_o} & 0 \end{bmatrix}, \qquad B_{\{+0\}} = \begin{bmatrix} \frac{1}{L} & 0 \\ 0 & 0 \\ 0 & \frac{-1}{C_o} \end{bmatrix} \tag{3.26}$$

$$A_{\{-0\}} = \begin{bmatrix} \frac{-R_{eq}}{L} & 0 & 0 \\ 0 & \frac{-R_L}{L_{load}} & \frac{1}{L_{load}} \\ 0 & \frac{-1}{C_o} & 0 \end{bmatrix}, \qquad B_{\{-0\}} = \begin{bmatrix} \frac{-1}{L} & 0 \\ 0 & 0 \\ 0 & \frac{-1}{C_o} \end{bmatrix} \tag{3.27}$$

$$A_{\{0+\}} = \begin{bmatrix} \frac{-R_{eq}}{L} & 0 & -\frac{1}{L} \\ 0 & \frac{-R_L}{L_{load}} & \frac{1}{L_{load}} \\ \frac{1}{C_o} & \frac{-1}{C_o} & 0 \end{bmatrix}, \qquad B_{\{0+\}} = \begin{bmatrix} 0 & 0 \\ 0 & 0 \\ 0 & \frac{-1}{C_o} \end{bmatrix} \tag{3.28}$$

$$A_{\{0-\}} = \begin{bmatrix} \frac{-R_{eq}}{L} & 0 & \frac{1}{L} \\ 0 & \frac{-R_L}{L_{load}} & \frac{1}{L_{load}} \\ \frac{-1}{C_o} & \frac{-1}{C_o} & 0 \end{bmatrix}, \qquad B_{\{0-\}} = \begin{bmatrix} 0 & 0 \\ 0 & 0 \\ 0 & \frac{-1}{C_o} \end{bmatrix} \tag{3.29}$$

$$A_{\{00\}} = \begin{bmatrix} \frac{-R_{eq}}{L} & 0 & 0 \\ 0 & \frac{-R_L}{L_{load}} & \frac{1}{L_{load}} \\ 0 & \frac{-1}{C_o} & 0 \end{bmatrix}, \qquad B_{\{00\}} = \begin{bmatrix} 0 & 0 \\ 0 & 0 \\ 0 & \frac{-1}{C_o} \end{bmatrix} \tag{3.30}$$

3.2.2 Duration of the TPS stages

Similarly to the SPS case, the control variable D affects the duration the converter spends in each stage. With the additional inputs D_1 and D_2, the order in which the converter moves through the stages is determined by these control variables as well.

The waveform for the primary side voltage v_p only depends on D_1. Its sign is initially $\{+\}$, before then moving through the other signs in the order shown in table 3.1.

Table 3.1: Time spent in each primary side voltage sign.

Time spent in stage	sign
$D_1 \frac{T}{4}$	$\{+\}$
$(1 - D_1) \frac{T}{2}$	$\{0\}$
$D_1 \frac{T}{2}$	$\{-\}$
$(1 - D_1) \frac{T}{2}$	$\{0\}$
$D_1 \frac{T}{4}$	$\{+\}$

The waveform for the secondary voltage v_s depends on both D and D_2. Unlike the primary side, the initial stage is not constant and depends on the relation between D and D_2 according to equation (3.31).

$$\begin{aligned} D_2 \geq D &\rightarrow \{+\} \\ D_2 < D &\rightarrow \{0\} \end{aligned} \tag{3.31}$$

These two different initial stages create two possible ways for the secondary voltage to move through its signs. These two possibilities are shown in Table 3.2.

Table 3.2: Time spent in each secondary sign.

$D_2 \geq D$	
Time spent in sign	sign
$(D + D_2)\frac{T}{4}$	$\{+\}$
$(1 - D_2)\frac{T}{2}$	$\{0\}$
$D_2\frac{T}{2}$	$\{-\}$
$(1 - D_2)\frac{T}{2}$	$\{0\}$
$(-D + D_2)\frac{T}{4}$	$\{+\}$

$D_2 < D$	
Time spent in sign	sign
$(D - D_2)\frac{T}{4}$	$\{0\}$
$D_2\frac{T}{2}$	$\{+\}$
$(1 - D_2)\frac{T}{2}$	$\{0\}$
$D_2\frac{T}{2}$	$\{-\}$
$(1 - D - D_2)\frac{T}{4}$	$\{0\}$

3.2.3 Order of the TPS stages

The number of unique stage orders that are possible needs to be computed to know how many models are needed to fully model the converter's TPS behavior. The boundary between two different stage orders is defined as when v_p and v_s change sign at the same time. An example of this is shown in Fig 3.17 where the control variable D_1 is changed from 0.3 to 0.7. This changes the order in which the stages are occurring from $\{+0\} \rightarrow \{00\} \rightarrow \{0+\} \ldots$ as seen in Fig 3.17a to the order shown in Fig 3.17b, which is $\{+0\} \rightarrow \{++\} \rightarrow \{0+\} \ldots$

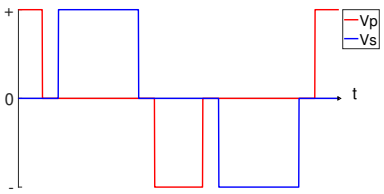

(a) $D = 1,\ D_1 = 0.3,\ D_2 = 0.5$

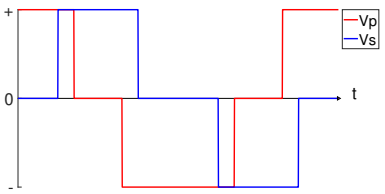

(b) $D = 1,\ D_1 = 0.7,\ D_2 = 0.5$

Figure 3.17: Primary and secondary voltage waveforms with two different stage orders.

This change occurs because v_p changes sign after v_s. These two changes are related to the first time expressions presented in Tables (3.1) – (3.2). The times when these two initial sign changes takes place (assuming that the primary side starts off with sign $\{+\}$) can be expressed as

$$t_p = D_1 \frac{T}{4}, \quad t_s = (D - D_2) \frac{T}{4}. \tag{3.32}$$

t_p and t_s represent when the primary and secondary voltage change their respective signs. By setting these two expressions equal to each other, the following expression dependent on D, D_1 and D_2

$$D = D_1 + D_2. \tag{3.33}$$

Equation (3.33) can be visualized in control-space as a plane that represents the boundary between two different stage orders. since all control variables have been normalized, the control-space is simply the unit cube. The plane defined by equation (3.33) has been visualized in Fig 3.18 which shows that the plane divides the control-space up into two polytopes where the order of the stages are different.

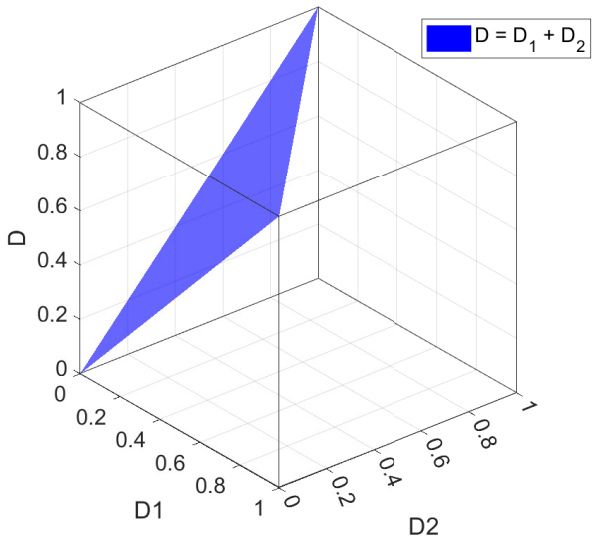

Figure 3.18: The boundary between two different stage orders defined by $D = D_1 + D_2$.

The same logic can be extended to all possible combinations of sign changes. These combinations consist of all possible ways of combining the times from Table 3.1 with the two lists of times presented in Table 3.2. This gives rise to 50 distinct time combinations, and thus planes, that can be visualized in control-space. Many of these combinations are however not possible, which is reflected by that their respective plane does not intersect the unit cube. For those constraints to change the order of the stages, the control variables would have to inhibit values outside the range of which they are defined. By analyzing these planes, there exist only 5 that intersect the unit cube. These planes are defined by

$$
\begin{aligned}
D &= D_1 - D_2 \\
D &= D_1 + D_2 \\
D &= 2 - D_2 - D_1 \\
D &= D_2 - D_1 \\
D &= D_2.
\end{aligned} \tag{3.34}
$$

By plotting the planes defined by equation (3.34), the control signal domain gets divided into 8 polytopes as visualized in Fig 3.19. Each polytope corresponds to a unique stage order, and the collection of these 8 polytopes defines every possible stage order with TPS modulation.

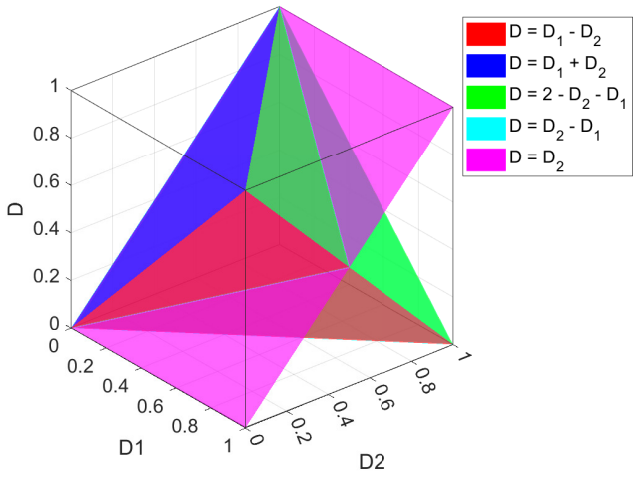

Figure 3.19: All boundary planes that intersect with the unit cube.

To model the TPS behavior, each polytope needs to be modeled. Each polytope is defined by its boundary planes, and any point P_i defined by equation (3.35) can be used to identify in which polytope P_1 through P_8 a point is located by the set of linear inequalities presented in equation (3.36).

$$
p = \begin{bmatrix} D \\ D_1 \\ D_2 \end{bmatrix}, \quad D \in [0,1], \quad D_1 \in [0,1], \quad D_2 \in [0,1] \tag{3.35}
$$

$$p = \begin{cases} P_1, & D \geq (D_1 + D_2) \\ P_2, & D \geq (2 - D_2 - D_1) \wedge (D \geq D_2) \\ P_3, & D \leq (D_1 - D_2) \wedge (D \geq D_2) \\ P_4, & D \geq (D_1 - D_2) \wedge (D \geq D_2) \wedge (D \leq D_1 + D_2) \wedge (D \leq 2 - D2 - D1) \\ P_5, & D \leq (D_2) \wedge (D \geq D_1 - D_2) \wedge (D \geq D_2 - D_1) \wedge (D \leq 2 - D_2 - D_1) \\ P_6, & D \leq (D_2 - D_1) \\ P_7, & D \geq (2 - D_2 - D_1) \wedge (D \leq D_2) \\ P_8, & D \leq (D_1 - D_2) \wedge (D \leq D_2) \end{cases} \tag{3.36}$$

A visual representation of equation (3.36) is shown in Fig 3.20, where the center of each polytope has been identified. Additionally, an exploded view of the polytopes is shown in Fig 3.21.

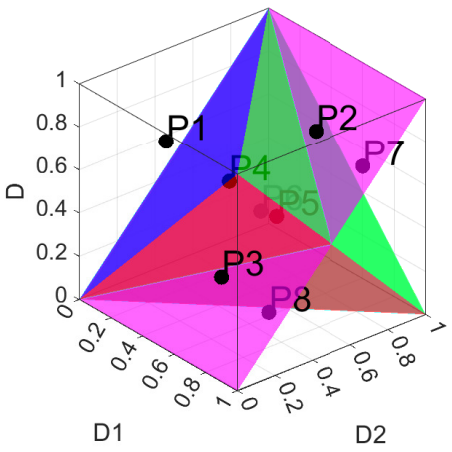

Figure 3.20: All polytopes defined by the boundary planes.

Figure 3.21: An exploded view of the polytopes.

With the stage order of all polytopes identified, the modeling of each polytope is done similarly to the SPS model, where each stage is discretized. The entire switching period is modelled by multiplying the previous state vector x_n by each consecutive stage, according to the corresponding polytope order presented in Table 3.3.

Table 3.3: Stage order for each polytope

	Stages								
Polytope	1	2	3	4	5	6	7	8	9
1	{+0}	{00}	{0+}	{00}	{−0}	{00}	{0−}	{00}	{+0}
2	{+0}	{++}	{0+}	{−+}	{−0}	{00}	{0−}	{+−}	{+0}
3	{+0}	{++}	{+0}	{00}	{−0}	{−−}	{−0}	{00}	{+0}
4	{+0}	{++}	{0+}	{00}	{−0}	{−−}	{0−}	{00}	{+0}
5	{++}	{0+}	{00}	{−0}	{−−}	{0−}	{00}	{+0}	{++}
6	{++}	{0+}	{00}	{0−}	{−−}	{0−}	{00}	{0+}	{++}
7	{++}	{0+}	{−+}	{−0}	{−−}	{0−}	{+−}	{+0}	{++}
8	{++}	{+0}	{00}	{−0}	{−−}	{−0}	{00}	{+0}	{++}

These polytopes give rise to a set of paths through the possible stages. An example of this, namely polytope 5, is displayed in Fig 3.22.

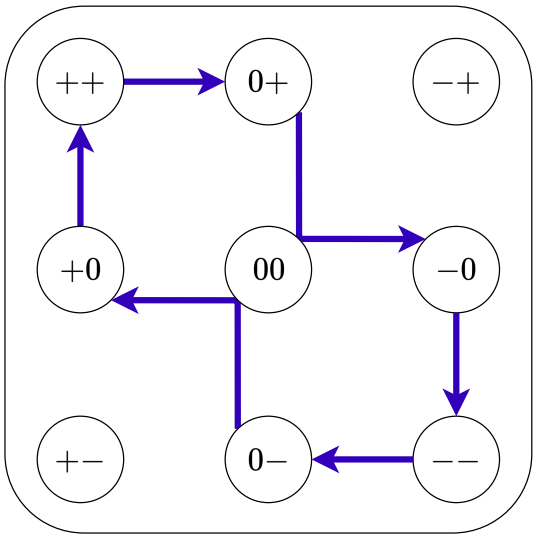

Figure 3.22: The order of the stages for polytope 5, with initial stage {++}.

The general way of computing the next state vector is shown in equation (3.37), where $\bar{A}_n$ and $\bar{B}_n$ corresponds to the A and B matrices related to the n:th stage in the polytope's list of stages.

$$\begin{aligned} x_{stage\_1} &= \bar{A}_1 x_n + \bar{B}_1 u \\ x_{stage\_2} &= \bar{A}_2(\bar{A}_1 x_n + \bar{B}_1 u) + \bar{B}_2 u \\ &\vdots \\ x_{n+1} &= \bar{A}_n(\bar{A}_{n-1}(\ldots(\bar{A}_1 x_n + \bar{B}_1 u) + \bar{B}_2 u) + \ldots + \bar{B}_{n-1} u) + \bar{B}_n u \end{aligned} \tag{3.37}$$

To create a model usable for controller design, the presented expression in equation

(3.37) which describes the relationship between x_{n+1} and x_n needs to be converted to state-space form. The n:th polytopes state dependency matrix A and input dependency matrix B can be extracted and expressed as shown in equations (3.38) and (3.39).

$$A_{P_n} = \bar{A}_1 \cdot \bar{A}_2 \cdot \bar{A}_3 \cdot \bar{A}_4 \cdot \bar{A}_5 \cdot \bar{A}_6 \cdot \bar{A}_7 \cdot \bar{A}_8 \cdot \bar{A}_9 \tag{3.38}$$

$$\begin{aligned} B_{P_n} = (&\bar{B}_8 + \\ &\bar{A}_8\bar{B}_7 + \\ &\bar{A}_8\bar{A}_7\bar{B}_6 + \\ &\vdots \\ &\bar{A}_8\bar{A}_7\bar{A}_6\bar{A}_5\bar{A}_4\bar{A}_3\bar{B}_2 + \\ &\bar{A}_8\bar{A}_7\bar{A}_6\bar{A}_5\bar{A}_4\bar{A}_3\bar{A}_2\bar{B}_1)u \end{aligned} \tag{3.39}$$

Using these matrices as shown in equation (3.40) will not provide usable controllers. This is because u, in this case, relates to the input voltage V_{in} and load disturbance i_{load}. The desired input vector consists of the three normalized phase shifts D, D_1, D_2 and the load disturbance i_{load}. Each $\bar{A}$ and $\bar{B}$ matrix inherit some dependency on D, D_1 or D_2 due to the discretization.

$$x_{n+1} = A_{P_n}x_n + B_{P_n}u \tag{3.40}$$

The D, D_1 and D_2 dependency of A_{P_n} and B_{P_n} is non-linear in D, D_1 and D_2. This makes the isolation approach made in the SPS case impossible in this case, due to the interdependency between the desired inputs. To capture the desired input behavior of the TPS controlled converter, A_{P_n} is evaluated, while B_{P_n} is linearized. This is done for a set of points in a 3D grid, with the linearization performed according to equations (3.41) and (3.42).

$$\bar{A}_{P_n} = A_{P_n}|_{\bar{u}_i}\,. \tag{3.41}$$

$$\begin{aligned}\bar{B}_{P_n} &= \underbrace{\left.\frac{\partial\left(B_{P_n}(u)V_{in}\right)}{\partial u}\right|_{\bar{u}_i}}_{B'_{P_n,i}}(u-\bar{u}_i) + B_d(\bar{u}_i)V_{in} \\ &= B'_{P_n,i}u - \underbrace{B'_{P_n,i}\bar{u}_i + B_d(\bar{u}_i)V_{in}}_{\substack{=\bar{E}_{P_n,i} \\ \text{Constant}}} \\ &= B'_{P_n,i}u - \bar{E}_{P_n,i} = \begin{bmatrix} B'_{P_n,i} & -\bar{E}_{P_n,i} \end{bmatrix} \begin{bmatrix} u \\ i_{load} \\ 1 \end{bmatrix}\end{aligned} \tag{3.42}$$

The linearized model enables controller design for each of the n polytopes, as it can be written on the form shown in equation (3.43).

$$x_{n+1} = \bar{A}_{P_n}x_n + \bar{B}_{P_n}\underbrace{\begin{bmatrix} D \\ D_1 \\ D_2 \\ i_{load} \\ 1 \end{bmatrix}}_{u'} \tag{3.43}$$

The number of parameter grid points used for the synthesized controller was selected as 3 points each for the parameters D, D_1 and D_2. This resolution ensures that there is at least one linearization point located in each polytope, except for polytopes 4 and 5. Increasing this resolution equally for D, D_1 and D_2 increases the number of points cubically, which poses a greater challenge in terms of implementation. Synthesizing controllers at higher parameter resolutions is more time intensive, and increasing the number of grid points puts a greater demand on available memory and computation power for implementation purposes. Keeping this resolution as small as possible is therefore vital. However, an insufficient amount of points leads to important dynamics being lost, since the dynamics for the polytopes differ.

For the final parameter V_{in}, only two points at the edges of the voltage range were chosen, located at $550\,V$ and $850\,V$. This limited resolution is deemed sufficient, as the input voltage has a linear effect on the B matrix. Ensuring that the controller interpolates between grid points captures the behavior of input voltages within the voltage range.

The model's accuracy was evaluated similarly to the SPS case, but with two more inputs. Frequencies at varying combinations were injected to the model, and their respective mean relative errors were computed at each point by comparing against the Simscape model. The results are visualized in Fig 3.23 as a 3D grid of points, with their color representing the relative errors. The figure visualizes the trend that

the model's accuracy is dependent on the difference in frequency between the main phase shift D and the two duty cycles D_1 and D_2.

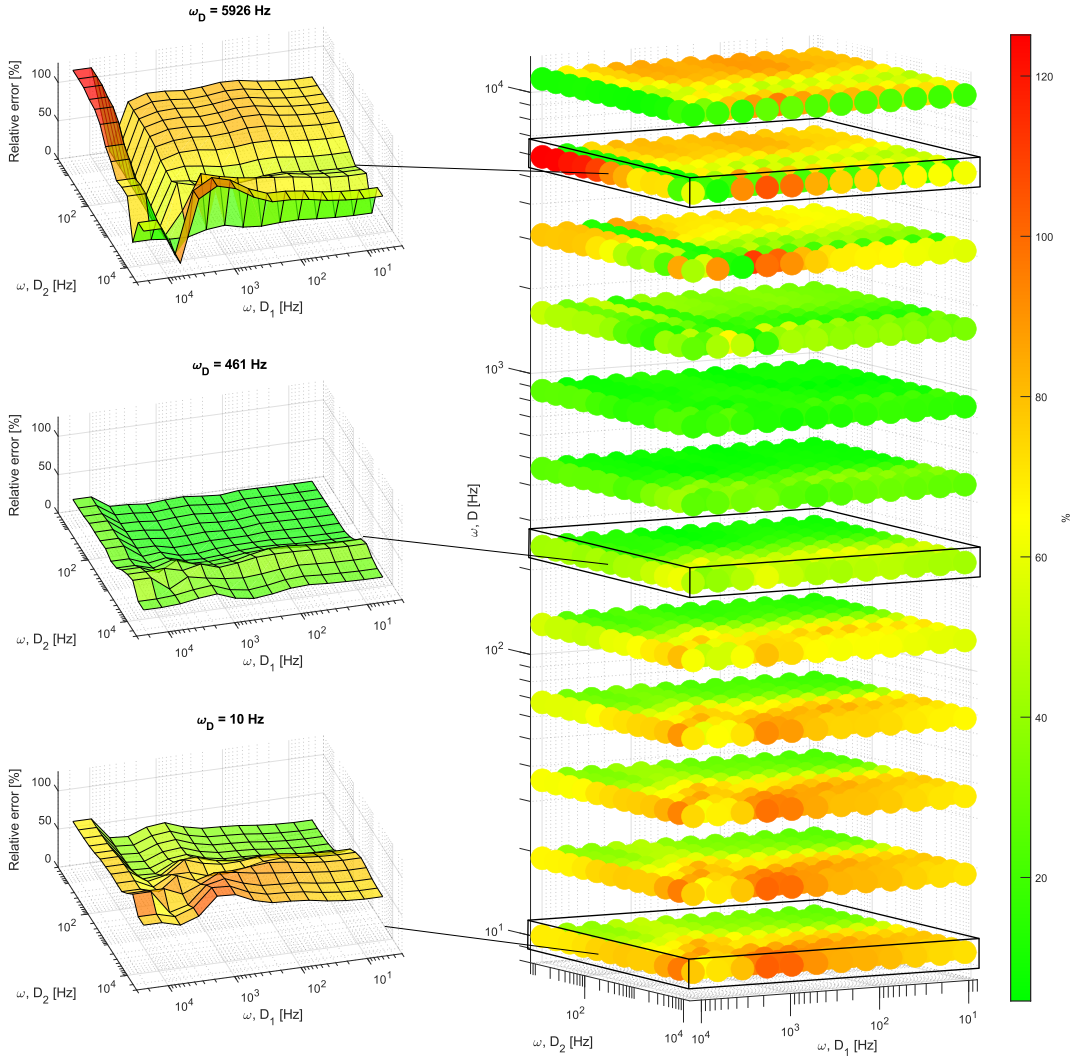

Figure 3.23: Individual layers of relative error, extracted from the cube.

4

Controller design

In this section, the creation of the three controllers is presented. The relevant structures and weights involved are also presented.

4.1 SPS PID

The PID controller was tuned using the input parametric model, rather than the linearized model, due to its higher accuracy. For synthesis, the MATLAB function `pidtune()` was used, which returns a PID controller based on an LTI model. Due to the non-adaptive behavior of such PID control, the input-parametric (varying) model was evaluated at average parameter values $\tilde{D} = 0.5$ and $V_{in} = 700\,\mathrm{V}$. This is to create a nominal model of the converter during SPS, from which the PID controller could be tuned. The resulting K_P, K_I and K_D values are shown in equation (4.1).

$$K_P = 0.0219, \quad K_I = 45.8500, \quad K_D = 7.6773 \cdot 10^{-7} \tag{4.1}$$

4.2 SPS LPV controller

To allow for robust controller synthesis, the elements of the Δ-P-K structure need to be selected. The generalized plant model P was designed as shown in Fig 4.1.

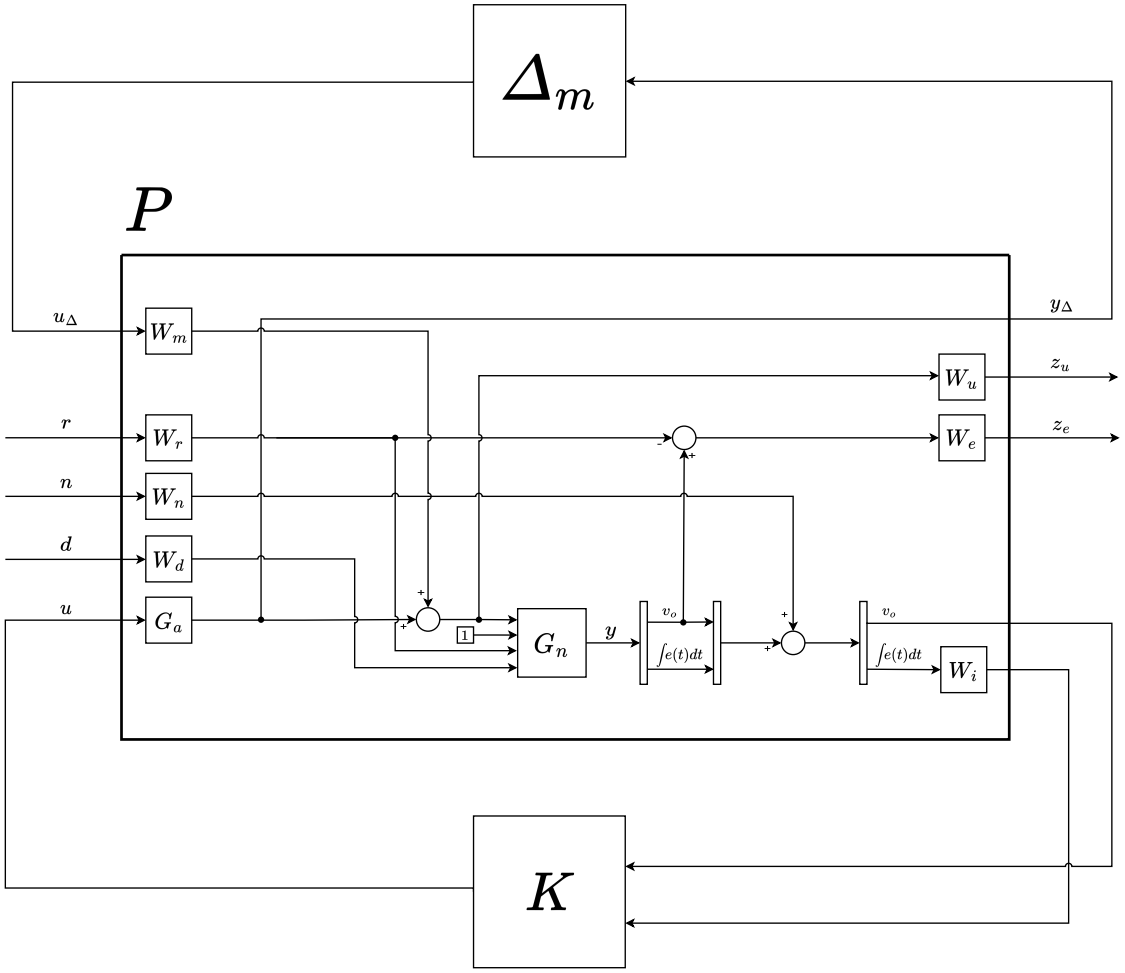

Figure 4.1: Δ-P-K structure of the SPS system.

The disturbance w consists of reference r, measurement noise n and load disturbance d (i_{load}). Performance metrics z_u and z_e depict the controller- and error performance respectively.

The weight W_e related to the tracking error was selected as a low-pass filter. This is because the controller should focus on reaching the steady state set by the reference, while high frequent errors should not be prioritized. This is because high-frequency errors perceived by the controller could be due to measurement noise or the voltage ripple from the modulation, and not due to poor tracking performance.

$$W_e = \frac{0.001s + 1005}{s + 100.5} \tag{4.2}$$

The weight W_r was used for additional tracking tuning. It is expressed as a low-pass filter, incentivizing the controller not to track with high-frequency.

$$W_r = \frac{1}{0.0003s + 1} \tag{4.3}$$

The weight W_u describes the penalty of control usage. It is set to a high constant gain, such that the controller will be conservative in its control signal usage. Making sure that the controller generates outputs within the range of D, D_1 and D_2 is crucial to minimize the need of saturation of control signals.

$$W_u = 1000 \tag{4.4}$$

The weight W_m describing model uncertainties was selected as high-pass filter. This is due to the fact that the model is less accurate at higher control signal frequencies, as shown in Fig 3.11. The transfer function was selected to capture the frequency-dependent error, with an additional factor.

$$W_m = \frac{0.9s^2 + 4816s + 1.289 \cdot 10^7}{s^2 + 5.077 \cdot 10^4 + 1.289 \cdot 10^9} \tag{4.5}$$

The weight G_a is describing the model's ability to affect the system, and was set to a constant gain to achieve similar results to W_u. It also incentives the controller to only generate control signals which do not violate the constraints put on the system.

$$G_a = 2 \tag{4.6}$$

The weight W_i is related to how the model feedbacks its integral error to the controller. It is is set to a constant gain, allowing for simple tuning of how much it should care about the integral error.

$$W_i = 100 \tag{4.7}$$

The weight W_d describes the model disturbances, and was selected as a constant gain. This is due to the load steps containing all frequencies.

$$W_d = 10 \tag{4.8}$$

The weight W_n is related to the measurement noise, and was selected as static gain. The measurement noise is expected to be a high frequency signal, but may include some bias. It is therefore modeled as a fixed value (2) for the measured

voltage. However, for the integral error, the low-pass nature of integration enables the controller to trust it to a higher degree.

$$W_n = \begin{bmatrix} 2 & 0 \end{bmatrix} \tag{4.9}$$

Given the weights and structure as shown above, the SPS controller was synthesized in MATLAB by using the function `lpvsyn()`.

4.2.1 TPS LPV controller

The structure of the TPS LPV controller is shown in Fig 4.2 where the weights for the TPS case are chosen with the same intentions as for the SPS case. This is due to the fact that both cases seek to achieve the same results, with the main difference being that more weights needs to be set for TPS. This is due to the extra control signals used by the TPS model, resulting in some weights becoming matrices of transfer functions.

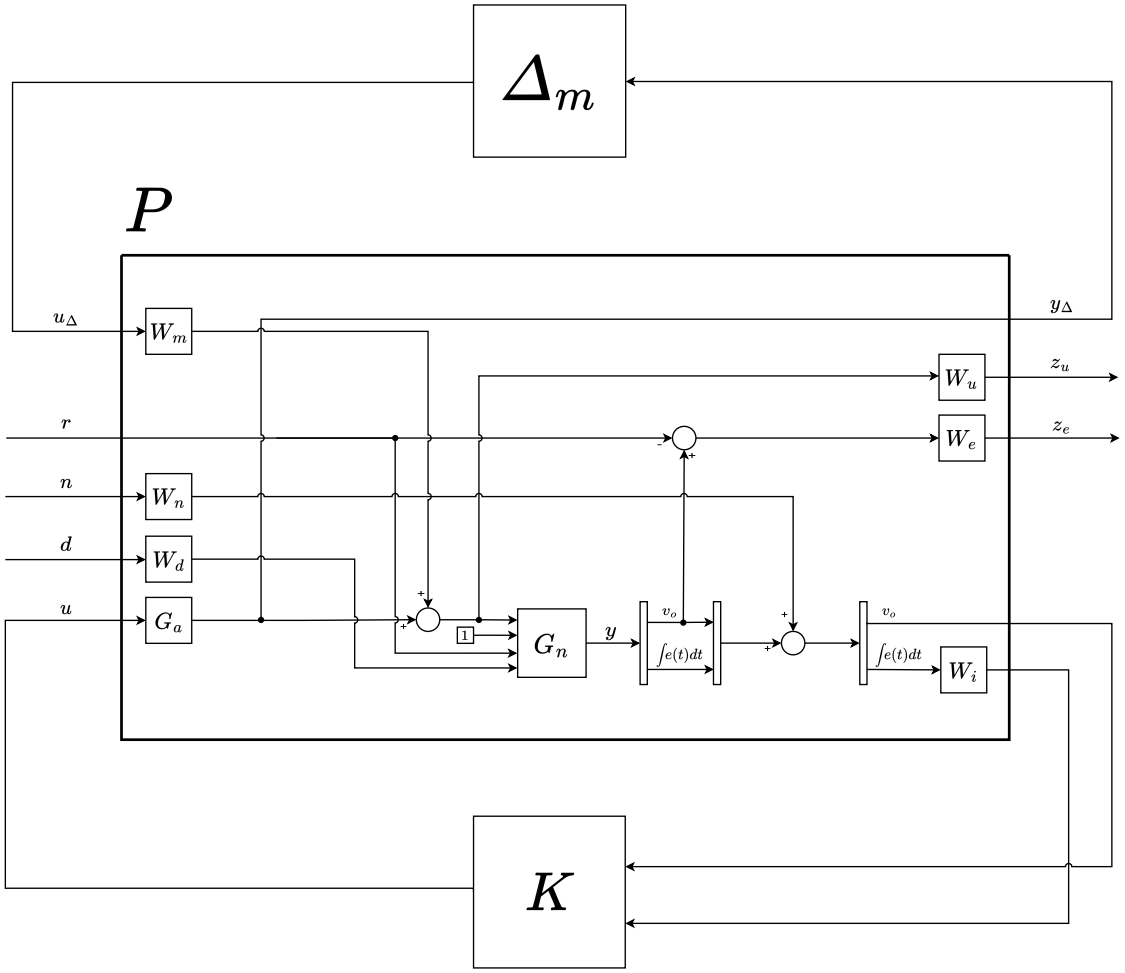

Figure 4.2: Δ-P-K structure of the TPS system.

The weights of W_e have been tuned based on the results from Fig 3.23.

$$W_e = \frac{0.001s + 100}{s + 0.1} \tag{4.10}$$

$$W_u = \begin{bmatrix} \frac{10s^2+2.083\cdot10^4s+2.169\cdot10^7}{s^2+6586s+2.169\cdot10^7} & 0 & 0 \\ 0 & \frac{10s^2+2.083\cdot10^4s+2.169\cdot10^7}{s^2+6586s+2.169\cdot10^7} & 0 \\ 0 & 0 & \frac{10s^2+2.083\cdot10^4s+2.169\cdot10^7}{s^2+6586s+2.169\cdot10^7} \end{bmatrix} \tag{4.11}$$

$$W_m = \begin{bmatrix} \frac{0.9s+257.7}{s+2.577\cdot10^4} & \frac{0.1s+810}{s+675} & \frac{0.1s+810}{s+675} \\ \frac{0.1s+810}{s+675} & 0.1 & \frac{0.9s+257.7}{s+2.577\cdot10^4} \\ \frac{0.1s+810}{s+675} & \frac{0.9s+257.7}{s+2.577\cdot10^4} & \frac{0.9s+257.7}{s+2.577\cdot10^4} \end{bmatrix} \tag{4.12}$$

$$G_a = \begin{bmatrix} \frac{1.25s+387.9}{s+646.6} & 0 & 0 \\ 0 & \frac{1.25s+387.9}{s+646.6} & 0 \\ 0 & 0 & \frac{1.25s+387.9}{s+646.6} \end{bmatrix} \tag{4.13}$$

$$W_i = 0.5 \tag{4.14}$$

$$W_d = 0.5 \tag{4.15}$$

$$W_n = \begin{bmatrix} 10 \\ 0.1 \end{bmatrix} \tag{4.16}$$

Given the weights and structure as shown above, the TPS controller was synthesized in MATLAB by using the function `lpvsyn()`.

4.2.2 Auxiliary controller features

The restrictions put on the control inputs severely affect the closed loop performance. The fact that D, D_1, and D_2 are all constrained to [0, 1] and rate limited to ± 0.2/sample, means that saturated control inputs are highly likely. With all controllers having some sort of integral action, such saturation can lead to integral windup.

To counter this, anti-windup can be added to the controllers. Simulink's PID block includes this feature, but it has to be implemented separately for both LPV controllers. For SPS LPV, there is only one controller output $u = D$ that can saturate.

During saturation (and/or rate limiting), the difference between raw- and restricted control input can be used to decrease the error (with gain K_{AW}) that the controller perceives. This way, the controller does not integrate an excessive amount of error when the control input is saturated. An illustration of this is displayed in Fig 4.3.

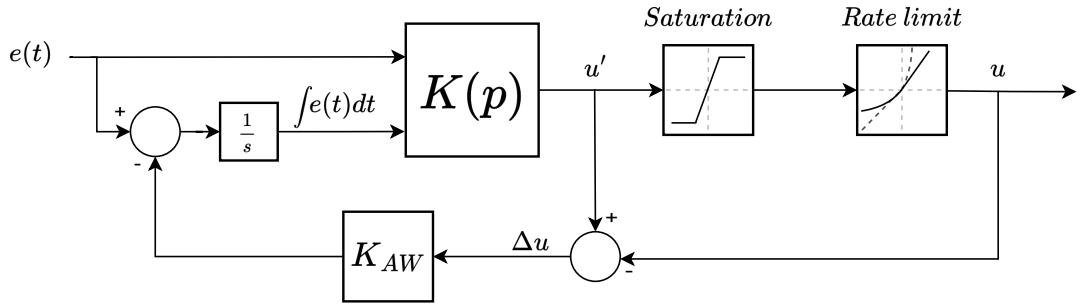

Figure 4.3: The implementation of anti-windup for the SPS LPV controller.

Anti-windup for the TPS LPV controller is more complicated due to its MIMO behavior ($u = [D\ D_1\ D_2]^T$). Instead of having merely one control input that can saturate, there are now three that can saturate and rate limit independently of each other. The solution in this thesis is built on a combination of all three. By computing the product of all saturation differences, scaling it with an anti-windup gain K_{AW}, and subtracting it from the error that is integrated, integral windup can be reduced. Additionally, a low-pass filter is added to prevent the feature from causing high-frequency oscillations. This concept is illustrated in Fig 4.4.

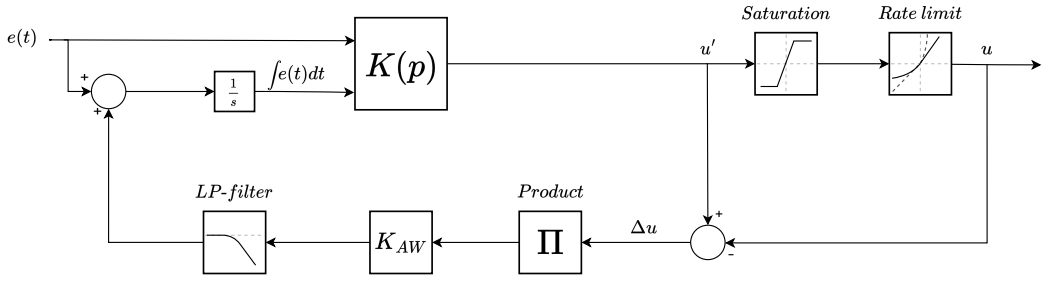

Figure 4.4: The implementation of anti-windup for the TPS LPV controller.

This implementation ensures that the anti-windup effect only activates once all the three control inputs are saturated, since if at least one is not, then the product becomes zero.

4.3 Evaluation

All tests will be performed with the converter and controller both operating at 25 kHz with the parameters shown in Table 4.1 and the input voltage set at 850 V.

Additionally, the Simscape circuit will be used as a plant, with 250 ns of dead-time. The performance of the controllers will be evaluated on how well they perform at voltage tracking, load regulation, and model uncertainties such as dead-time.

Table 4.1: Component values.

Component	Value
R_{in}	0.05 Ω
R_{MSF}	$13.5 \cdot 10^{-3}$ Ω
R_{trafo}	0.0414 Ω
R_L	10 Ω
C_o	$120 \cdot 10^{-6}$ F
L_{mag}	$2 \cdot 10^{-3}$ H
L_{load}	10^{-3} H
$L_{leakage}$	$3.6 \cdot 10^{-5}$ H

4.3.1 Performance metrics

The performance metrics for voltage tracking are

- Rise time [ms]
- Overshoot [%]
- Settling time (time to reach steady state within 4 V of voltage reference) [ms],

while the metrics for disturbance rejection are

- Maximum deviation [% of current voltage]
- Settling time (time to reach steady state within 4 V of current voltage) [ms].

The specified 4 V range for the settling time metric is based on the voltage ripple of the converter. At steady state, the only deviations from the reference are induced by the saw-tooth like waveform of the voltage. Selecting 4 V as the threshold will therefore give a metric on how fast the controllers are able to pull the voltage to the reference at steady state.

Voltage tracking refers to the controllers' ability to control the output voltage to track a given reference voltage. Each controller will be given a voltage reference to follow, and their performance will be evaluated using the performance metrics.

Load regulation refers to how well the controller is able to keep the desired output voltage in the presence of load disturbances. each controller will be simulated, and load steps will be applied to the system and their performance will be evaluated using the performance metrics.

Due to the nature of dynamic controllers, there will be an initial time in the simulations without any disturbances or voltage steps. This is to ensure that all controllers reach steady state. The time $t = 0$ ms in the plots refers to when the scenario starts, not when the simulations are started. The scenario in question is displayed in Fig 4.5.

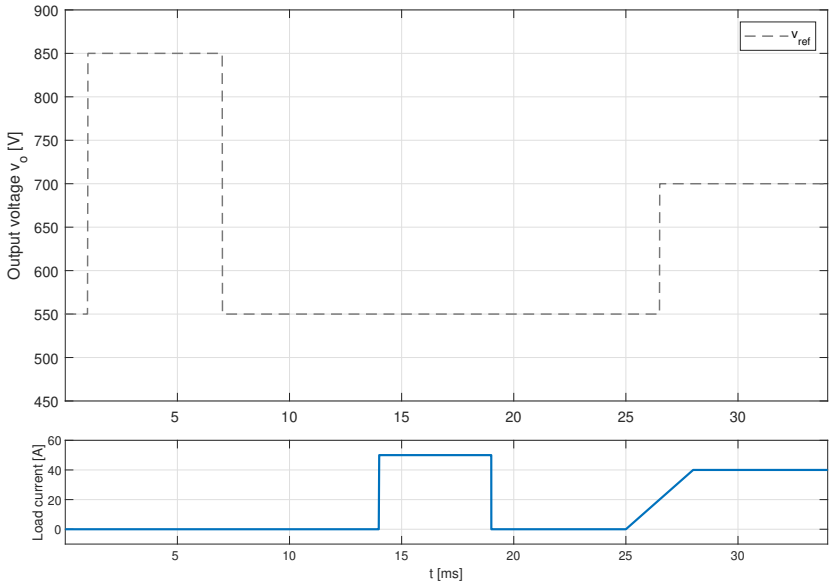

Figure 4.5: The voltage tracking and current load scenario.

It features the following:

- A voltage reference step from minimum- (550 V) to maximum voltage (850 V).
- A 50 A current load step at 550 V (combined with the nominal load to achieve the maximum power of 30 kW).
- A voltage reference step from 550 V to 700 V during a load current ramp of 13 000 A/s, up to 40 A.

5

Results

In this chapter, the results are presented. The entire simulation will be shown, as well as the individual parts and their performance metrics.

5.1 Tracking and load regulation

The entire simulation is displayed in Fig 5.1.

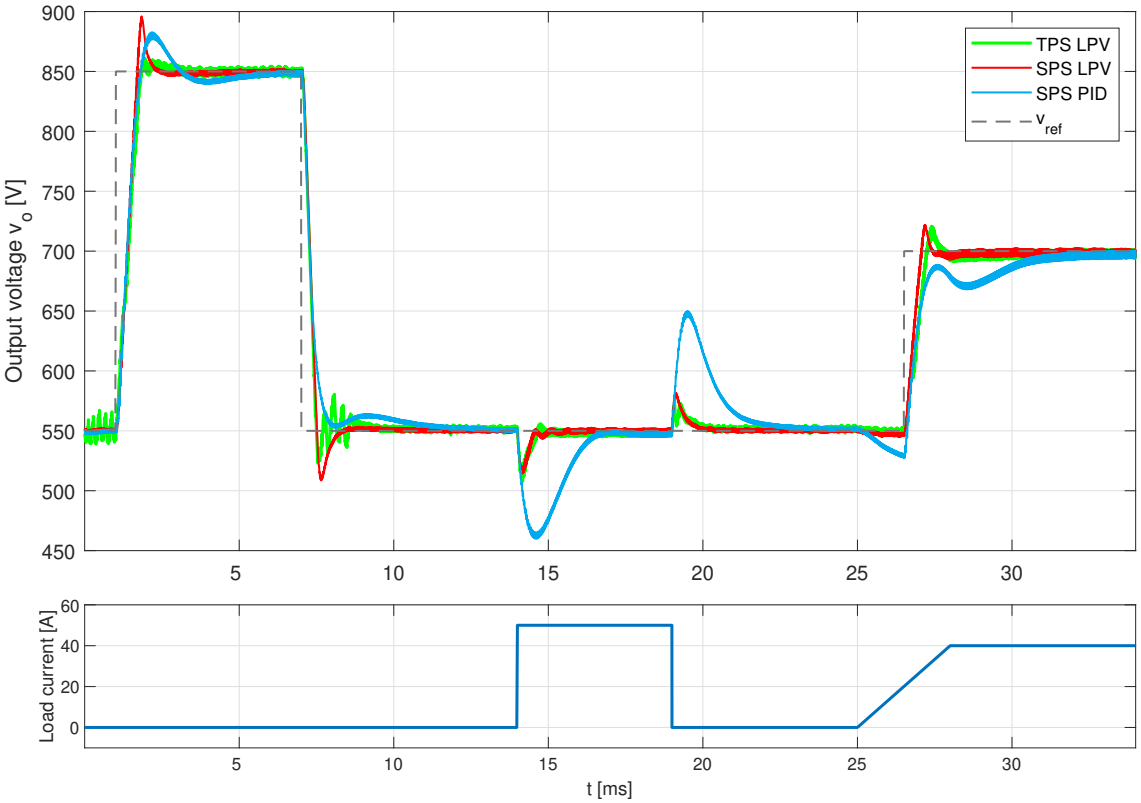

Figure 5.1: The complete tracking simulation with all controllers.

The first reference voltage step is shown in Fig 5.2, and the performance metrics in table 5.1. Note the short settling time for the LPV controllers, and the low overshoot

for TPS LPV.

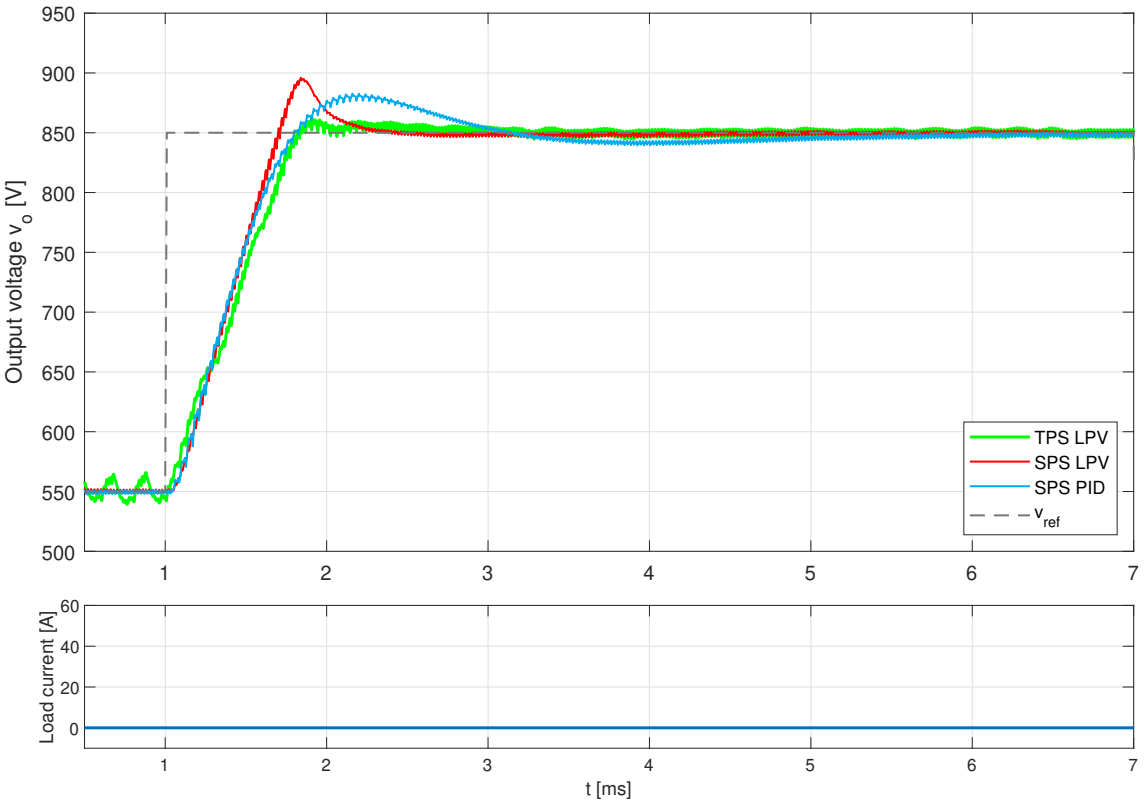

Figure 5.2: The controllers' performance during the first voltage step.

Table 5.1: Performance metrics for the first voltage step

Controller	Rise time [ms]	Overshoot [%]	Settling time [ms]
TPS LPV	0.59	3.83	2.14
SPS LPV	0.51	15.3	1.87
SPS PID	0.57	10.7	4.39

The second step in voltage is displayed in Fig 5.3, and its metrics in table 5.2. The overshoot of the SPS LPV and the oscillations of the TPS LPV are clearly visible.

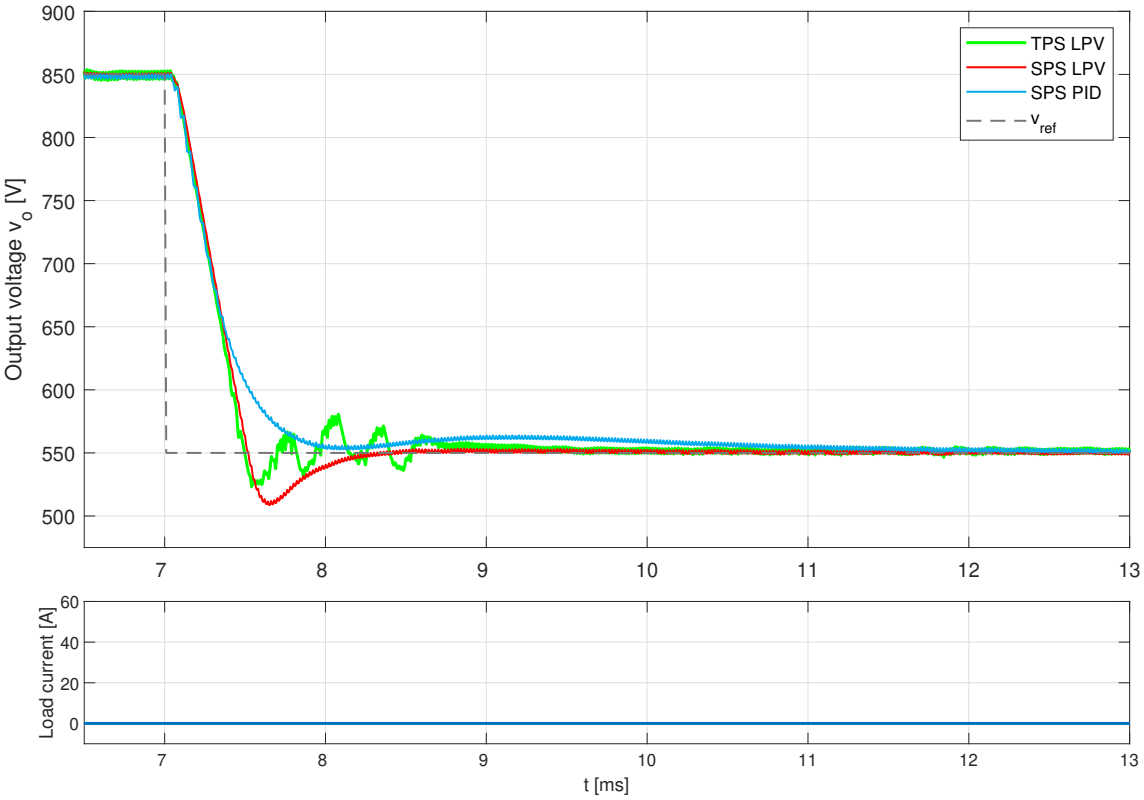

Figure 5.3: The controllers' performance during the second voltage step.

Table 5.2: Performance metrics for the second voltage step.

Controller	Rise time [ms]	Overshoot [%]	Settling time [ms]
TPS LPV	0.34	8.74	2.53
SPS LPV	0.35	13.3	1.29
SPS PID	0.53	N/A	4.79

The load regulation is shown in Fig 5.4, and its metrics in tables 5.3 and 5.4. Note the high voltage deviations for SPS PID.

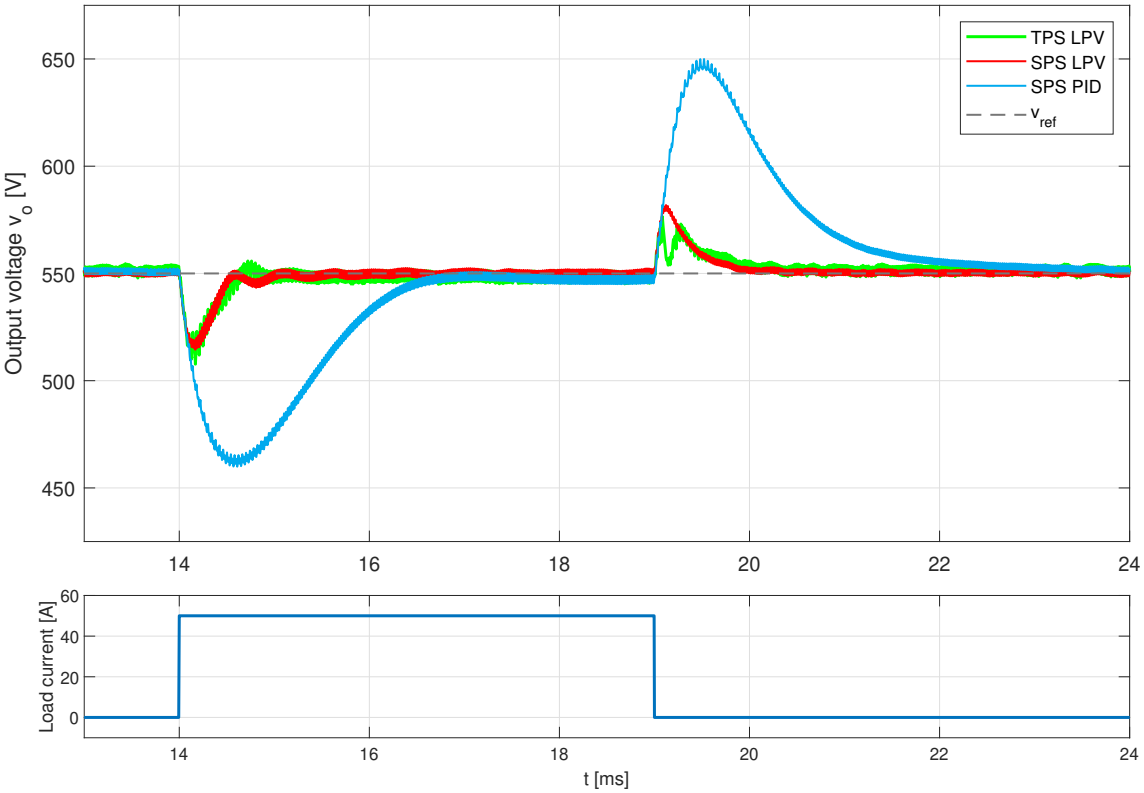

Figure 5.4: The controllers' performance during the steps in load current.

Table 5.3: Performance metrics for the step-up in load current.

Controller	Maximum deviation [%]	Settling time [ms]
TPS LPV	7.64	1.07
SPS LPV	6.44	0.96
SPS PID	16.4	2.70

Table 5.4: Performance metrics for the step-down in load current.

Controller	Maximum deviation [%]	Settling time [ms]
TPS LPV	4.82	1.09
SPS LPV	5.80	0.84
SPS PID	18.08	3.98

Finally, the last step in reference voltage during a ramp in load current is displayed in Fig 5.5, and its metrics in table 5.5. Notice that the SPS PID is severely affected by the load ramp, while it is minimal for the LPV controllers.

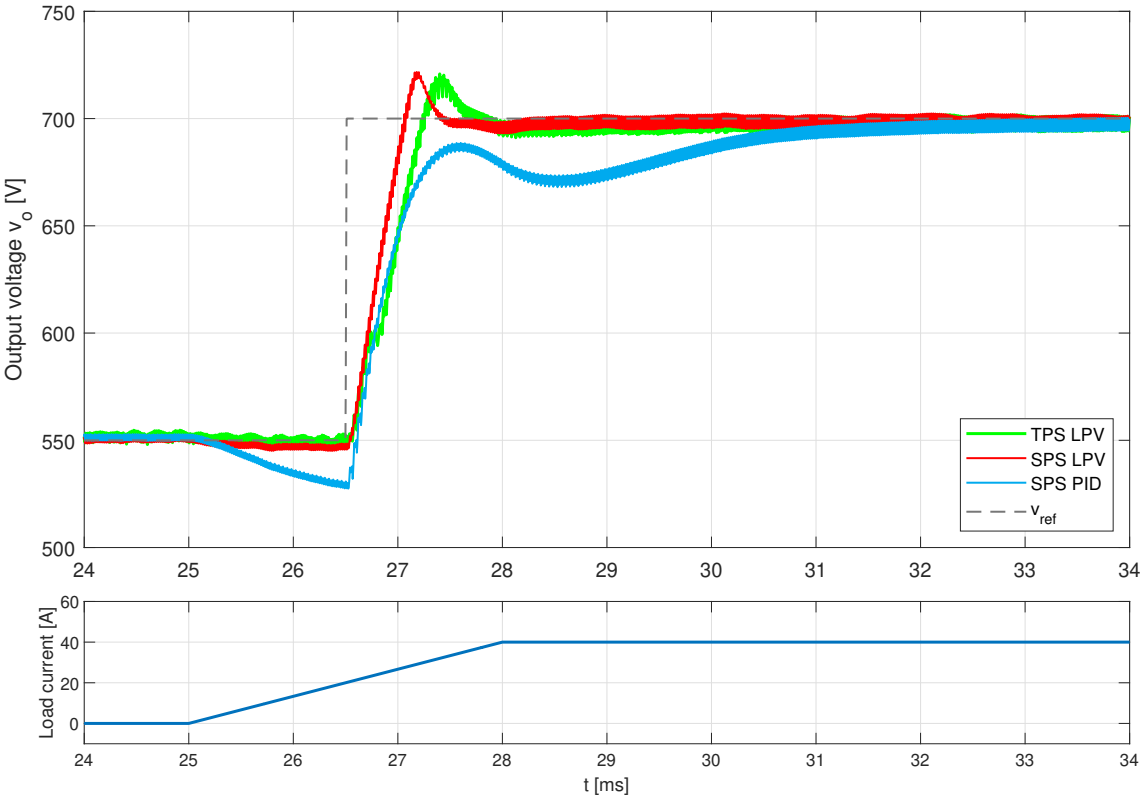

Figure 5.5: The controllers' performance during the final step in reference voltage.

Table 5.5: Performance metrics for the step-up in load current.

Controller	Rise time [ms]	Overshoot [%]	Settling time [ms]
TPS LPV	0.56	14.1	1.17
SPS LPV	0.40	14.4	0.86
SPS PID	0.77	N/A	4.11

6

Discussion

One of the most significant findings in this thesis is how the highly non-linear behavior of the converter could be modeled as a set of LTI systems scheduled by the previously used control inputs, resulting in a model usable for control design. The assumption that previous control inputs can be used as parameters used in the model to describe the converters' dynamics does inherently cause the models' accuracy to become dependent on the control signals' rate of change. This dependency was shown to not be simply increasing with frequency, some other factor does cause model errors for the system, which can be seen in Fig 3.11 as the peak located around 100 Hz. Further investigation needs to be conducted to understand this local frequency dependent model discrepancy.

The two LPV controllers were consistently outperforming the PID controller in all performed test scenarios, for most performance metrics. The LPV controllers provide significantly faster voltage tracking and load disturbance rejection when compared to the PID controller. The PID controller does in some cases provide results with less overshoot than the two LPV controllers, these cases are however followed by significantly slower settling times. Both LPV controllers also manage to fully reject the ramped disturbance shown in Fig 5.5, whereas the PID controller does not manage to adequately react, resulting in a significant voltage dip.

The SPS LPV and TPS LPV controllers provide similar performance. The main difference being that the TPS controller manages to step from 550V to 850V without overshoot in the first voltage step, as seen in Fig 5.2. The TPS controller's ability to both quickly increase the voltage and transition into keeping a constant voltage without overshoot is most likely doe to its ability to utilize all three possible control variables to control the output voltage. Further tuning is possible, as the final test scenario visualized in Fig 5.5 shows a slight overshoot when tracking the output voltage during a load disturbance.

The TPS controller shows unwanted oscillatory behavior, mainly visible in Fig 5.3. This behavior could be caused due to the fact that the model does not take dead-time into consideration, while the actual plant does operate with it. Another possibility is that the LPV behavior causes the controller to fluctuate as the control variables change. Futhermore, the linearization (and parameter-) resolution of 3 points per

control variable and 2 for the input voltage may not be enough. This limited resolution might not be sufficient to capture the dynamics at all possible operating points without the risk of causing oscillations in the output voltage.

The performance gained with robust LPV for DAB converters may not be sufficiently high considering the complexity of such controllers. Not only are the TPS LPV and SPS LPV controllers cumbersome in terms of synthesis, but also in implementation. Increasing the number of grid points may increase model accuracy, but also puts a greater burden on the computers that run the control loop. Converters frequently utilize embedded control systems, which are often limited in both computing power and available memory. This severely limits the order- and number of grid points of LPV controllers due to the required computations per control loop iteration. For each controller output calculation, matrix interpolation, matrix multiplication and matrix addition will have to be performed due to the dynamic LPV controller behavior. This is not an issue for PID controllers, since they only have to store three static parameters (K_p, K_i, and K_d) and perform simple computations in comparison.

The usage of PID control could very likely improve. Tuning of the PID controller was performed using the MATLAB function `pidtune()`. Such functions may be unbiased, but could arguably produce better performing controllers given the optimal tuning conditions. Additionally, the plant model fed to the function was an LTI system sampled from the LPV model at average parameter values. The fact that the PID performed the way it did, given the simplicity of the model used for synthesis, shows that advanced control methods are not necessarily essential for DAB converters. Furthermore, PID control does not suffer from oscillations caused by parameter variations. One could therefore argue that the controller parameters K_p, K_i, and K_d themselves are more stable compared to the LPV controllers' parameters.

7

Conclusion

This thesis has presented how the performance of model-based robust LPV controllers compare against PID controllers when tasked with voltage tracking and disturbance rejection. The results show that the model-based controllers outperformed the PID in both SPS and TPS operation. The difference in implementation efforts, memory usage and computation power needed to get these model-based controllers to run on real hardware is however considerably higher than the relatively simple implementation of a PID.

The approximations and simplifications made during the modeling of the converter for both the SPS and TPS case proved to be sufficiently accurate such that controllers could be designed after their dynamics. Knowing that the modeling assumptions made are valid assumptions allows for future work to expand the model. For instance, modeling the losses of the converter, which would allow for more efficient controllers to be synthesized.

The implementation of robust model-based controllers does allow for future controllers that can operate with some level of uncertainty, which potentially allow for converters to be built with components with larger uncertainties or for converters to be able to operate for longer where other controllers might fail due to component properties changing over time

An interesting aspect to examine through future work could be how the number of linearization points affect the performance of the controllers. Knowing this information would allow for more informed decisions being made regarding the trade-off between controller performance and memory usage.

Furthermore, additional future work is to evaluate such controllers in hardware. Mere simulations of the converter running Robust LPV control does not take computational power into account. Hardware implementation would then give an idea of how much performance is required from the embedded systems, as well as how much memory is needed.

Bibliography

[1] X. Li, D. Lepour, F. Heymann, and F. Maréchal, "Electrification and digitalization effects on sectoral energy demand and consumption: A prospective study towards 2050," *Energy*, vol. 279, p. 127 992, 2023, ISSN: 0360-5442. DOI: https://doi.org/10.1016/j.energy.2023.127992. [Online]. Available: https://www.sciencedirect.com/science/article/pii/S0360544223013865.

[2] T. Kohama, Y. Sogawa, and S. Tsuji, "Optimized on-off control to improve efficiency of paralleled converter system," in *2014 IEEE 36th International Telecommunications Energy Conference (INTELEC)*, 2014, pp. 1–7. DOI: 10.1109/INTLEC.2014.6972181.

[3] R. M. Burkart and J. W. Kolar, "Comparative η– ρ– σ pareto optimization of si and sic multilevel dual-active-bridge topologies with wide input voltage range," *IEEE Transactions on Power Electronics*, vol. 32, no. 7, pp. 5258–5270, 2017. DOI: 10.1109/TPEL.2016.2614139.

[4] D. Das and K. Basu, "Optimal design of a dual-active-bridge dc–dc converter," *IEEE Transactions on Industrial Electronics*, vol. 68, no. 12, pp. 12 034–12 045, 2021. DOI: 10.1109/TIE.2020.3044781.

[5] S. S. Khan and H. Wen, "Universal sensorless open-circuit fault detection and isolation method of dual-active-bridge converters with low-cost diagnostic circuit," *IEEE Transactions on Power Electronics*, vol. 37, no. 11, pp. 13 652–13 667, 2022. DOI: 10.1109/TPEL.2022.3182382.

[6] R. K. Kanaparthi, J. P. Singh, and M. S. Ballal, "A review on multi-port bidirectional isolated and non-isolated dc-dc converters for renewable applications," in *2022 IEEE International Conference on Power Electronics, Drives and Energy Systems (PEDES)*, 2022, pp. 1–6. DOI: 10.1109/PEDES56012.2022.10080049.

[7] X. Ma, A. Tong, B. Li, L. Hang, G. Li, and P. Shen, "Zvs operation of dab converter based on triple-phase-shift modulation scheme with optimized inductor current," in *IECON 2017 - 43rd Annual Conference of the IEEE Industrial Electronics Society*, 2017, pp. 4702–4707. DOI: 10.1109/IECON.2017.8216810.

[8] M. R. Mehdi and A. Mahmood, "Robust control of full bridge dc-dc converter," in *2016 2nd International Conference on Robotics and Artificial Intelligence (ICRAI)*, 2016, pp. 99–104. DOI: 10.1109/ICRAI.2016.7791236.

[9] F. Krismer, "Modeling and optimization of bidirectional dual active bridge dc–dc converter topologies," Available at https://doi.org/10.3929/ethz-a-006395373, PhD thesis, Technische Universität Wien, Wien, AU, 2010.

[10] F. Zhou, X. Zhang, P. Rao, Q. Zhang, J. Cao, and P. Luo, "Dead-time effect and efficiency improvement of the high power dual active bridge dc-dc converter with series resonant," in *2019 IEEE Vehicle Power and Propulsion Conference (VPPC)*, 2019, pp. 1–6. DOI: 10.1109/VPPC46532.2019.8952300.

[11] T. Glad and L. Ljung, *Control theory: Multivariable and Nonlinear Methods*. Taylor & Francis Group, 2000.

[12] S. Skogestad and I. Postlethwaite, *Multivariable feedback control: Analysis and Design*. Hoboken, US-NJ: John Wiley, 2005.

[13] A. Hjartarson, P. Seiler, and A. Packard, "Lpvtools: A toolbox for modeling, analysis, and synthesis of parameter varying control systems," *IFAC-PapersOnLine*, vol. 48, no. 26, pp. 139–145, 2015, 1st IFAC Workshop on Linear Parameter Varying Systems LPVS 2015, ISSN: 2405-8963. DOI: https://doi.org/10.1016/j.ifacol.2015.11.127. [Online]. Available: https://www.sciencedirect.com/science/article/pii/S240589631502385X.

[14] A. Tong, L. Hang, G. Li, and J. Xu, "Equivalent circuit model of dual active bridge converter," in *IECON 2017 - 43rd Annual Conference of the IEEE Industrial Electronics Society*, 2017, pp. 4677–4682. DOI: 10.1109/IECON.2017.8216806.

[15] I. The MathWorks, *Symbolic math toolbox*, Natick, Massachusetts, United State, 2019. [Online]. Available: https://www.mathworks.com/help/symbolic/.

[16] The MathWorks, Inc., *Simscape electrical*, [Online; accessed Feb 2024], 2024-02. [Online]. Available: https://se.mathworks.com/help/sps/index.html.

DEPARTMENT OF ELECTRICAL ENGINEERING
CHALMERS UNIVERSITY OF TECHNOLOGY
Gothenburg, Sweden
www.chalmers.se

CHALMERS
UNIVERSITY OF TECHNOLOGY